Impurity analysis of JET DiMPle pulses

K D Lawson[1,4,*] ⓘ, I H Coffey[1,2,4], F Rimini[1,4], I Książek[3,4] and JET Contributors[5]

[1] UKAEA/CCFE, Culham Science Centre, OX14 3DB Abingdon, United Kingdom
[2] Astrophysics Research Centre, School of Mathematics and Physics, Queen's University Belfast, BT7 1NN Belfast, United Kingdom
[3] Institute of Physics, Opole University, Pl. Kopernika 11, 45-040 Opole, Poland
[4] EUROfusion Consortium, JET, Culham Science Centre, OX14 3DB Abingdon, United Kingdom

E-mail: Kerry.Lawson@ukaea.uk

CrossMark

Abstract
Divertor monitoring pulses (DiMPle) have been run in JET from the C35 campaign onwards. They provide an opportunity to study the impurity contamination of the plasma when it is limited by different surfaces within the machine, as well as the longer term behaviour of the impurities. In these discharges the plasma is first limited on the outer wall, then on the inner wall and, subsequently, in the X-point configuration the outer strike point is positioned on the horizontal tile 5 of the machine followed by tile 6 and then the vertical tile 7. The present study details the impurity behaviour in the DiMPle pulses from JET-ILW campaigns C35 to C38, which ran from 2015 to 2019. The impurities can largely be divided into two groups. The first, including most gases, are present immediately after their use in the machine; the second group includes those elements that are retained on plasma facing surfaces within the vessel. Most of these are metals, for which a systematic behaviour is found. Influxes due to metallic dust particles behave more like the elements of the first group. The origin of the impurities where this is known is given as well as details of the systematic behaviour, including differences due to the line-of-sight of the observing spectrometer. A clear difference is seen when the discharge fuel is H and this has implications for tritium and deuterium-tritium operations.

Keywords: impurities, JET-ILW, tokamaks, long-term impurity behaviour, behaviour on Plasma Facing Surfaces

(Some figures may appear in colour only in the online journal)

1. Introduction

Impurity behaviour in plasma machines is best considered as a series of special cases, each depending on the previous history and the plasma configuration, as well as plasma parameters, such as density and temperature, which influence both the release and transport of impurities into the bulk plasma. The previous history will determine the background impurity levels in the machine and the plasma configuration, particularly the position of the plasma relative to plasma facing surfaces, is critical in that it affects the release of impurities either from the surface element itself or contaminants previously deposited on these surfaces. In general, the only impurity for which a clearly reproducible behaviour can be found is for the element of the plasma facing surfaces that has a low atomic number, Z. In JET this element was C during the earlier JET-C campaigns, for which an overview is given by Romanelli and Laxåback (2011). In the 2009/2011 shutdown an ITER-like wall was installed in JET, with ~4000 tiles being replaced by remote handling (Matthews et al 2007). The new

[5] See the author list of Joffrin et al (2019 Nucl. Fusion **59** 112021).
[*] Author to whom any correspondence should be addressed.

tiles were manufactured from Be, W, W coated CFC and Be coated Inconel, with the W tiles being sited in the divertor and the Be tiles forming the main chamber walls of the machine. A comparison of the JET plasma operations with the metal wall and the previous C machine is given by Matthews *et al* (2013). Differences in the impurity behaviour are discussed by Coenen *et al* (2013). The JET-ILW campaigns have allowed JET to contribute to an understanding of plasma operations with an ITER relevant mix of impurities (Matthews *et al* 2014), with Litaudon *et al* (2017) giving an overview of the JET results up to that date. More recently Joffrin *et al* (2019) describes the preparations being carried out on JET for the first deuterium-tritium operations with an ITER-like wall.

The most important low-Z impurity in these later campaigns is Be and, as with C, the emission is found to be reproducible. Monitoring the intensity of a line from the highest ionization stage seen in the spectrum during the limiter phase of a discharge aids analyses of the stability of the VUV spectrometer sensitivity used in their observation. Other impurities are found to have a more variable emission that needs to be assessed for the particular pulses being studied. In monitoring impurity behaviour it is essential to compare similar pulses; the divertor monitoring pulses (DiMPle) used on JET to assess the contamination of particular plasma facing surfaces are ideal for this purpose.

In a DiMPle pulse the plasma is positioned on five different surfaces within the JET machine. Initially a limiter configuration is used with the plasma touching the outer and then inner walls at 6.0–6.5 s and 7.3–7.8 s, respectively. This is followed by an X-point configuration with the outer strike point positioned on the X-point tiles 5, 6 and 7 at 13.5–14.0 s, 20.0–20.5 s and 23.5–24.0 s, respectively. Tile 5 and 6 are horizontal tiles on the divertor floor, with tile 5 being more central and made from bulk W. Tile 7 is an outer vertical tile. Tiles 6 and 7 are constructed from W coated CFC. The plasma configurations are shown in figures 1–3 and the plasma parameters of typical DiMPle pulses with and without additional heating, in this case neutral beam injection (NBI), in figure 4. They have been run from the start of the JET campaign C35, with table 1 giving information about the JET campaigns covered by this analysis. Before this the impurity behaviour in the JET machine was assessed using Be monitoring pulses, in which, as with the DiMPle pulses, the same configuration and plasma parameters were used (Brezinsek *et al* 2013). A list of DiMPle pulses with a brief comment for each is given at:- https://users.euro-fusion.org/tfwiki/index.php/DiMPle.

The present analysis describes the impurity behaviour in the DiMPle pulses from campaign C35 (August–December 2015) to C38 (May 2018–December 2019), this including the hydrogen campaign, C37 (June–September 2016), which due to the lower fuel mass might be expected to lead to different impurity levels. In C38 there were two periods when He was used as the fuel, pulses 93023–93089 and pulses 93847–93908. The analysis uses passive VUV spectroscopic data recorded with three of the JET survey spectrometers. This spectral region is especially valuable for such studies in that its spectral features most closely match the importance of particular elements occurring in the plasma and all impurity elements found in plasmas
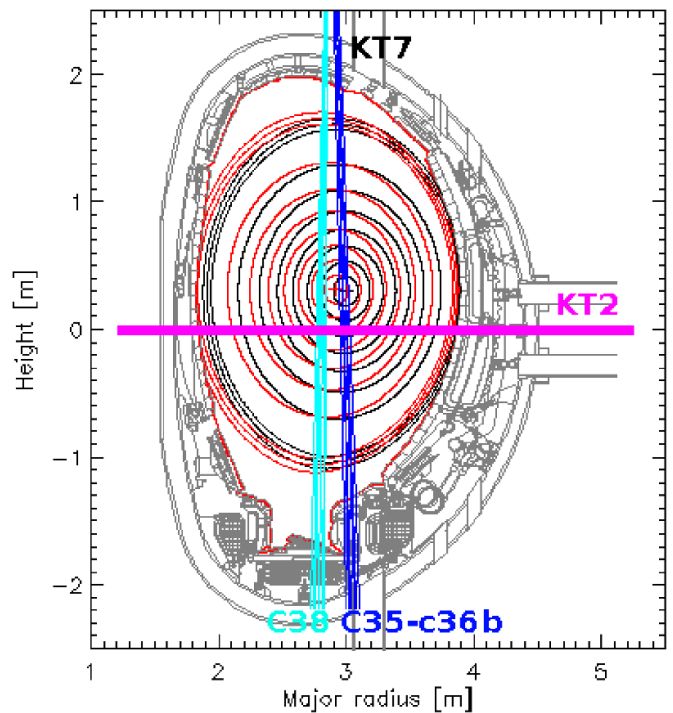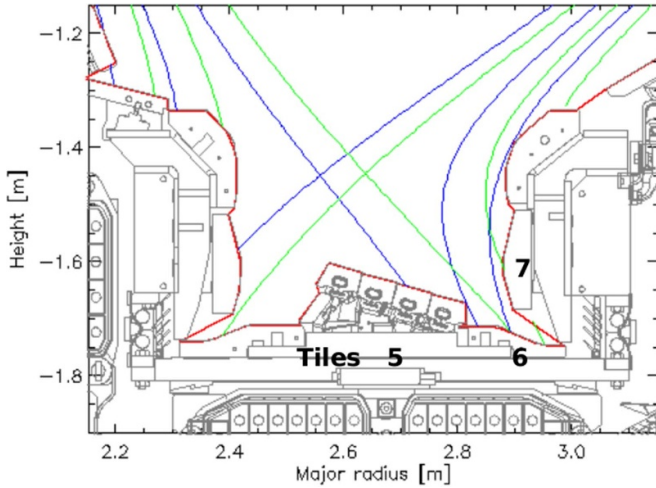

Figure 1. Magnetic configuration of the outer (6.25 s) (in black) and inner wall (7.54 s) (in red) phases of the DiMPle pulse 91779. The KT2 and KT7 lines-of-sight are shown.
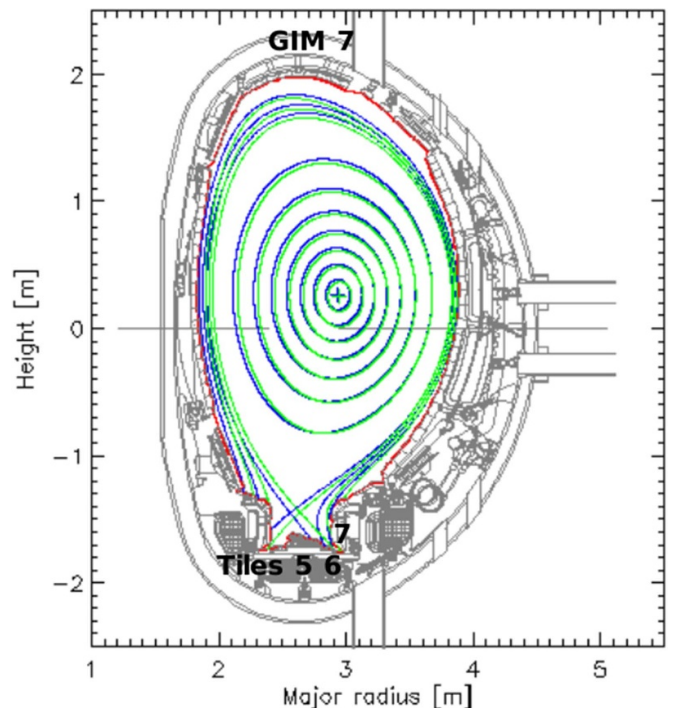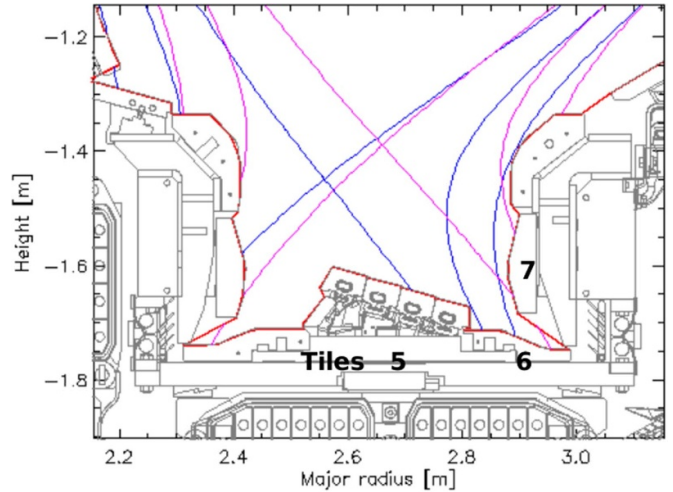

Figure 2a. Magnetic configuration of the DiMPle pulse 91779 X-point phases with the outer strike point on tile 5 (13.75 s) (in blue) and tile 6 (20.25 s) (in green).

with keV temperatures have features falling in this region. The visible observations of these plasmas generally only include emission from low ionization stages of the low-Z elements. They therefore tend to be indicative of the impurity behaviour

Figure 2b. Magnetic configuration in the divertor of the DiMPle pulse 91779 X-point phases with the outer strike point on tile 5 (13.75 s) (in blue) and tile 6 (20.25 s) (in green).
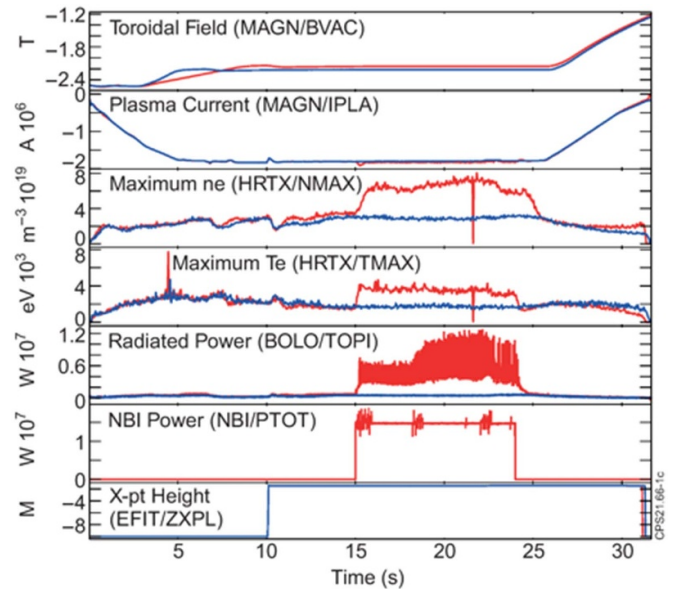

Figure 3b. Magnetic configuration in the divertor of the DiMPle pulse 91779 X-point phases with the outer strike point on tile 5 (13.75 s) (in blue) and tile 7 (23.77 s) (in magenta).
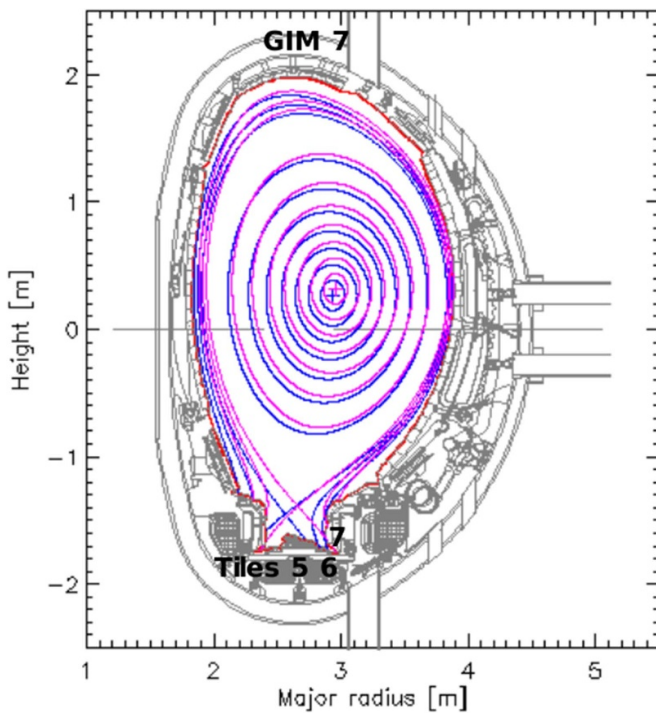
Figure 3a. Magnetic configuration of the DiMPle pulse 91779 X-point phases with the outer strike point on tile 5 (13.75 s) (in blue) and tile 7 (23.77 s) (in magenta).

Figure 4. Plasma parameters of Ohmic DiMPle pulse 91779 (in blue) and with NBI, pulse 92155 (in red).

2. Spectroscopic analysis

Although VUV spectra, more so than those in either the visible or soft x-ray spectral regions, give an immediate indication of the occurrence and importance of an element in a plasma with keV temperatures, the relationship between the line intensities and the concentration or power radiated by the element is complex. Consequently, line intensities are used for the present study, rather than concentrations or elemental components of radiated power for which there would be a much greater uncertainty. The similarity of the DiMPle discharges allows comparisons to be made between pulses, although, apart from the mid-Z elements Cr to Cu, there is no direct correlation between

in the scrape-off layer (SOL) more than the core plasma, often measuring impurity influxes, which depend critically on the line of sight and whether this views the impurity source. Visible spectra give little information about mid- and high-Z elements, which emit mainly in the VUV and soft x-ray spectral regions.

Table 1. JET campaigns.

Campaign	Dates	Pulse numbers	Fuel	Comments
C35	26 August 2015–18 December 2015	88084–89472	D	D NBI, KT7 viewing divertor throat.
C36	11 January 2016–20 May 2016	89476–90797	D	D NBI, Break in operations before pulses 89828 and 90761.
C37	28 June 2016–2 September 2016	90806–91756	H	D and H NBI (see figure 23).
C36b	28 September 2016–15 November 2016	91757–92504	D	D NBI.
C38	3 May 2018–20 December 2019	92671–96563	D/He	D NBI, KT7 LOS moved to view divertor, two periods when He fuel used.

the measured intensities for different elements and concentrations or radiated power components. This is due to the wide range of Z of the impurity elements found in JET plasmas making it necessary to use different atomic transitions, whose radiation is emitted from very different plasma regions. For the mid-Z elements the same transition can be used resulting in the intensities being proportional to concentrations and elemental components of radiated powers. Nevertheless, this proportionality is approximate in that the emission is still from somewhat different plasma regions with their different densities and temperatures.

That all elements radiate in the VUV region creates a particular difficulty in the analysis of spectra recorded with the usual spectrometers available for surveying the VUV spectrum on large plasma machines in that the spectrum is extremely crowded. Supposing a similar energy density of lines to that found in the visible spectral region (~4000–8000 Å), which covers a factor of two in energy range, the VUV, usually defined as from ~50 or 100–2000 Å, covers an energy range of a factor of 20 or 40. Despite this, only one or two survey spectrometers are normally used. If the assumption regarding the energy density is valid for low-Z elements, it does not apply to higher Z elements, for which a far higher number of transitions fall in the VUV spectral region. For example, in the spectral range ~70–320 Å there are ~70 spectral lines of varying intensities due to each of Ni, Cu, Fe and Cr, the mid-Z elements seen routinely or reasonably often in JET plasmas (Lawson and Peacock 1980). More recently it has been necessary to add Mo, Ti and Cl to this list of mid-Z elements. Fortunately, the spectrum of these elements is dominated by six particularly intense lines belonging to the Li-, Be-, Na- and Mg-like ionization stages, at least making a precise monitoring of these elements possible.

The three VUV spectrometers used in the present analysis are known locally as KT2, KT7/2 and KT7/3. They are situated at the same toroidal location (Octant 6) on the JET machine. KT2 is a SPRED spectrometer (Fonck *et al* 1982) with a horizontal line-of-sight along the vessel mid-plane (shown in figure 1). It has a spectral resolution of ~5 Å and a spectral range of ~100–1000 Å. The spectra for pulse 92155 averaged between 6.0 and 6.5 s is shown in figure 5. The KT7 instruments have the same vertical line-of-sight, which for campaigns C35 to C36b viewed the throat of the outer divertor, but which at the beginning of C38 was moved to observe the

divertor emission directly. Both lines-of-sight are illustrated in figure 1. KT7/2 is also a SPRED instrument (Wolf *et al* 1995); its higher spectral resolution of ~1 Å is of particular value given the complexity of the VUV spectra, although this instrument has a more limited spectral range of only 140–444 Å. Figure 6 shows the KT7/2 spectrum corresponding to that of figure 5. KT7/3 is a Schwob-Fraenkel instrument (Schwob *et al* 1987) with a single detector, which has been set to observe the W unresolved transition arrays (UTAs) at wavelengths of ~42–70 Å. There is a tendency for heavy elements such as W to move outboard due to a centrifugal force (Wesson 1997, Koskela *et al* 2015), which can result in their peak emission falling outside either of the KT7 lines-of-sight used. This makes a cross-check of the recorded KT7 W behaviour with the horizontally viewed KT2 W feature observed between wavelengths of ~140 and 260 Å essential. The KT2 W feature again consists of a number of overlapping UTAs from similar and somewhat lower ionization stages than those observed by KT7/3.

3. Results

A study is made of the impurity behaviour observed when the plasma touches different plasma facing surfaces in the JET machine recorded in the C35 to C38 DiMPle pulses. The similarity of these pulses provides conditions under which the long term development of impurities can also be studied. This has been done by following the spectral line intensities of characteristic lines of the most common impurity elements found in JET, namely He, Be, C, N, O, Ne, Cl, Ar, Ti, Cr, Fe, Ni, Cu, Kr, Mo and W. Very occasional observations of other impurity elements have not been included in this analysis.

If the complexities of the VUV spectrum resulting from the density of lines found in this spectral region makes the analysis of a single pulse difficult, the problem of providing a reliable analysis is more severe when data from a large number of pulses is routinely accessed as in the present case. In such an analysis it is essential to include all the elements likely to occur in the plasma so as to account for all possible blends that could affect the reliability of the measurements. A number of intense lines characteristic of particular elements had to be rejected because of blending. For a number of other lines, checks on the intensities of possible blended lines were made, the observation being rejected if the blended line was expected to make
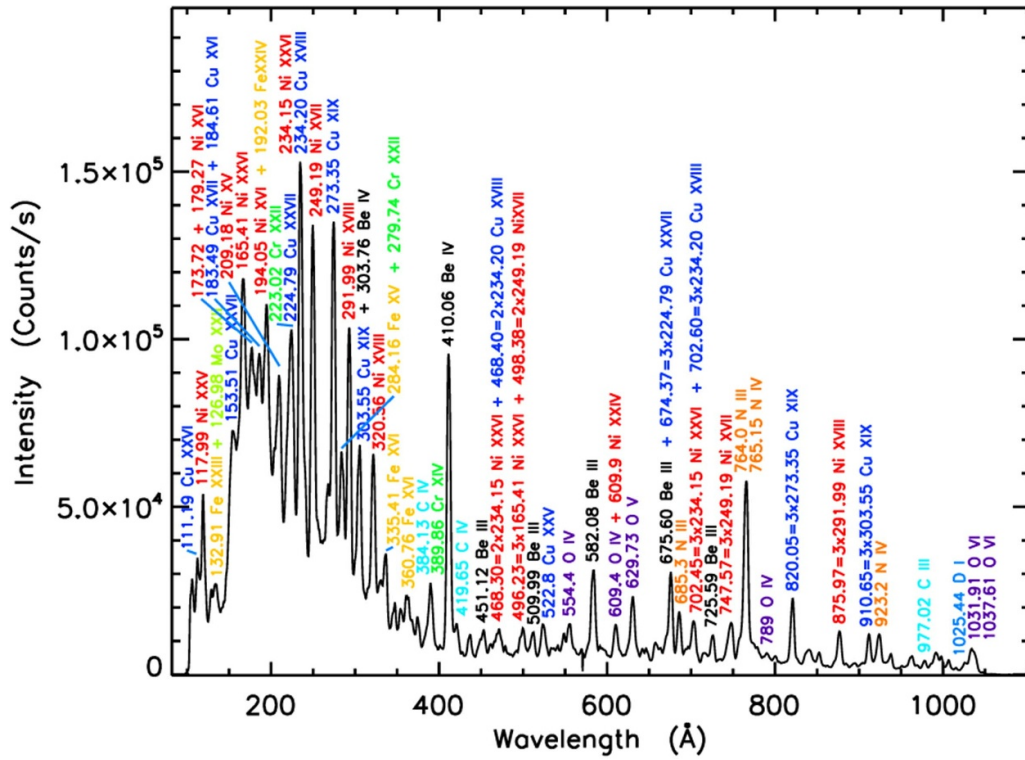
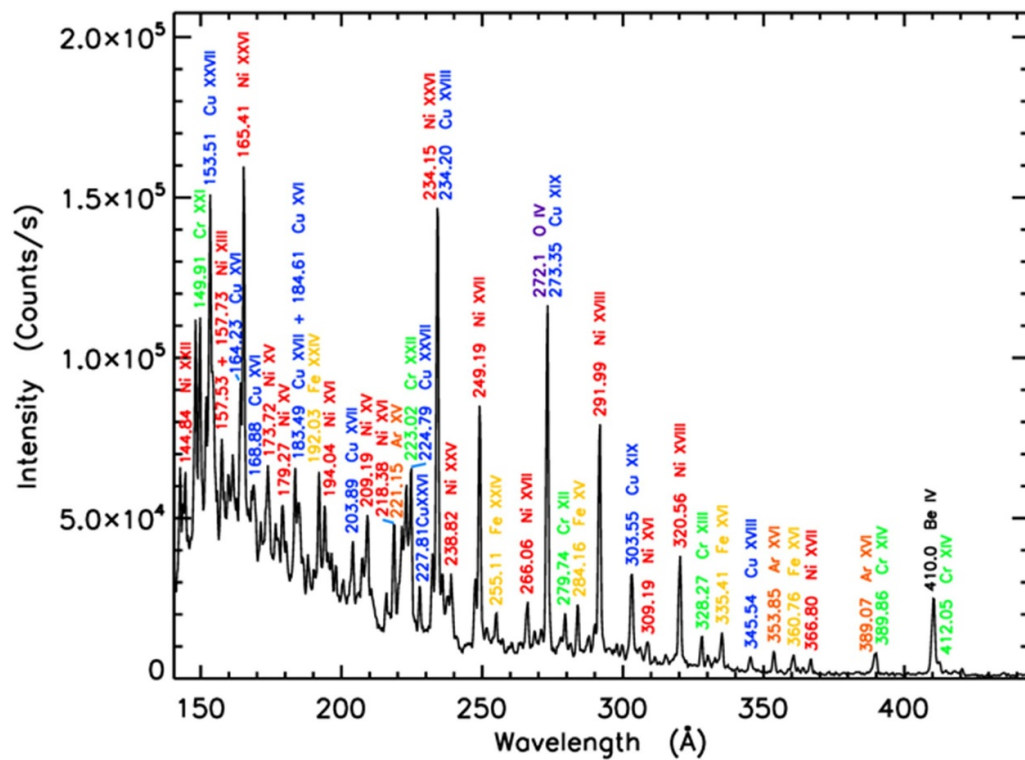**Figure 5.** KT2 spectrum of pulse 92155 averaged between 6.0 and 6.5 s.

Figure 6. KT7/2 spectrum of pulse 92155 averaged between 6.0 and 6.5 s.

Table 2. Spectral lines used to monitor impurities.

Ionization stage	Wavelength (Å)	Spectrometer	Identification	Comment
He II	303.78	KT2	1s-2p	Blend with Be IV and Cu XIX
He II	303.78	KT7/2	1s-2p	Blend with Be IV and Cu XIX
Be IV	410.06	KT2	2-3	
Be IV	410.06	KT7/2	2-3	
C III	977.02	KT2	$2s^2$-2s2p	
C IV	312.43	KT2	2s-3p	
C IV	312.43	KT7/2	2s-3p	
N IV	923.06/3.22	KT2	$2s2p$-$2p^2$	
O V	629.73	KT2	$2s^2$-2s2p	
O V/VI	172.17/2.94/3.08	KT7/2	$2s^2$-2s3p/2p-3d	
Ne VIII	780.32	KT2	$2s\ ^2S_{1/2}$-$2p\ ^2P_{1/2}$	
Cl XIV	237.70	KT7/2	$2s^2\ ^1S_0$-$2s2p\ ^1P_1$	Blend with He II
Cl XV	415.50	KT7/2	$2s\ ^2S_{1/2}$-$2p\ ^2P_{1/2}$	Blend with Ne V/adjust peak pixel to improve reliability
Ar XV	221.15	KT7/2	$2s^2\ ^1S_0$-$2s2p\ ^1P_1$	
Ar XVI	353.85	KT2	$2s\ ^2S_{1/2}$-$2p\ ^2P_{3/2}$	
Ar XVI	353.85	KT7/2	$2s\ ^2S_{1/2}$-$2p\ ^2P_{3/2}$	
Ti XIX	169.58	KT7/2	$2s^2\ ^1S_0$-$2s2p\ ^1P_1$	Ensure significantly greater than W background and both Ti lines observed
Ti XX	259.29	KT7/2	$2s\ ^2S_{1/2}$-$2p\ ^2P_{3/2}$	Ensure significantly greater than W background and both Ti lines observed
Cr XIII	328.27	KT7/2	$3s^2\ ^1S_0$-$3s3p\ ^1P_1$	
Cr XIV	389.86	KT7/2	$3s\ ^2S_{1/2}$-$3p\ ^2P_{3/2}$	Blend with Ar XVI
Fe XVI	335.41	KT7/2	$3s\ ^2S_{1/2}$-$3p\ ^2P_{3/2}$	
Ni XVIII	291.99	KT2	$3s\ ^2S_{1/2}$-$3p\ ^2P_{3/2}$	
Ni XVIII	291.99	KT7/2	$3s\ ^2S_{1/2}$-$3p\ ^2P_{3/2}$	
Cu XIX	273.35	KT2	$3s\ ^2S_{1/2}$-$3p\ ^2P_{3/2}$	Blend with O IV
Cu XIX	273.35	KT7/2	$3s\ ^2S_{1/2}$-$3p\ ^2P_{3/2}$	
Kr XXVI	178.99	KT7/2	$3s\ ^2S_{1/2}$-$3p\ ^2P_{3/2}$	Ensure significantly greater than W background
Mo XXXII	127.87	KT2	$3s\ ^2S_{1/2}$-$3p\ ^2P_{3/2}$	Neighbouring Mo XXXI and Fe XXIII lines
Mo XXXII	176.65	KT7/2	$3s\ ^2S_{1/2}$-$3p\ ^2P_{1/2}$	Ensure significantly greater than W background
W UTA	165–253	KT2	W XV–W XXXVI	Includes non W line emission
WIK	(176 + 201)/2–142	KT2	W XV–W XXXVI	Reduces the effect of non W line emission
W UTA	42–54	KT7/3	W XXV–W XLVI	

too great a contribution to the total intensity. Table 2 lists the wavelengths of the lines used in the analysis with their identifications. Those lines for which constraints were imposed are indicated in this table. A minimum intensity has been set for each line as judged by its appearance in the spectra of a number of pulses; below this intensity the measurement is not considered a reliable indication of the monitored element.

The UTAs of W observed in the KT2 and KT7/3 spectrum have been monitored by a simple integration of the spectrum between wavelengths of 147–213 Å and 42–54 Å, respectively, with a background subtraction defined by these wavelengths. The KT2 measurement integrated in this way includes interfering lines due to other elements. Since these can be intense, a new analysis of the KT2 W spectrum has led to an alternative measurement that largely avoids the contamination of these other lines. This alternative uses the average of integrations centred on wavelengths of 176 and 201 Å covering a range of −5 to +5 pixels, with a background subtraction of the integrated area about a wavelength of 142 Å, this with the same integration range. This measure is denoted WIK. Further information regarding the choice of spectral lines for each element is given by Lawson and Coffey (2020).

The following sections describe the observations for the individual elements with a summary given in table 3. For clarity, guide lines are given in some of the diagrams. Since the data presented here is a subset of that accessed in the full analysis, it is noted that the guide lines are also indicative of the behaviours seen for similar impurity elements that have not been illustrated here. The full analysis is presented by Lawson and Coffey.

3.1. Helium

He is observed by both the KT2 and KT7/2 spectrometers (figures 7 and 8, respectively). It has been used in JET mainly as a minority gas in ion cyclotron resonance heating (ICRH) experiments, particularly from pulse 90028 in the C36 campaign. Large excursions, which decay rapidly, are seen immediately after its use, this being particularly evident in C38 after

Table 3. Summary of impurity behaviours.

Element	Observation	LOS effect	Wall phases	X-point phases
He	Edge	Yes	Large excursions from background level after use of He Inner wall higher for KT2 Few KT7/2 observations	Large excursions from background level after use of He KT7/2 (less so KT2) tile6 and tile7 > tile5
Be	Edge/core	—	Used as sensitivity stability check	Levels generally lower than wall phases
C	Edge	Yes	KT7/2 outer > inner with KT2 showing the reverse	KT7/2 tile6 > tile7 > tile5 KT2 tile5 > tile6 and tile7
N	Edge	—	Large excursions after N experiments, but no obvious bias	Large excursions after N experiments, but no obvious bias
O	Edge	Yes	KT7/2 outer > inner with KT2 showing the reverse	KT7/2 tile6 > tile7 and tile5 KT2 tile5 > tile6 and tile7
Ne	Edge	—	No obvious bias	Tile5 tends to be highest, particularly after pulse ∼94200
Cl	Core	Only KT7/2, although as Ar	Highest emission at start of campaigns Outer > inner	Highest emission at start of campaigns, tile6 > tile7 > tile5
Ar	Core	No	Outer > inner	Tile5 > tile6 and tile7
Ti	Core	No	Five outer, one inner, background levels	One tile5, five tile6, five tile7, all influxes
Cr	Core	No	Outer ≫ inner	Tile6 > tile7 > tile5
Fe	Core	No	Outer ≫ inner	Tile6 > tile7 > tile5
Ni	Core	No	Outer ≫ inner	Tile6 > tile7 > tile5
Cu	Core	No	Outer ≫ inner	Tile6 > tile7 > tile5
Kr	Core	—	Three outer, two inner influxes	Five tile5, one tile6, two tile7, one influx, other background levels
Mo	Core	No	Mainly outer	Limited data, tile6 > tile7 > tile5
W	Edge/Core	No	Outer > inner	Small separation, with tile6 marginally higher
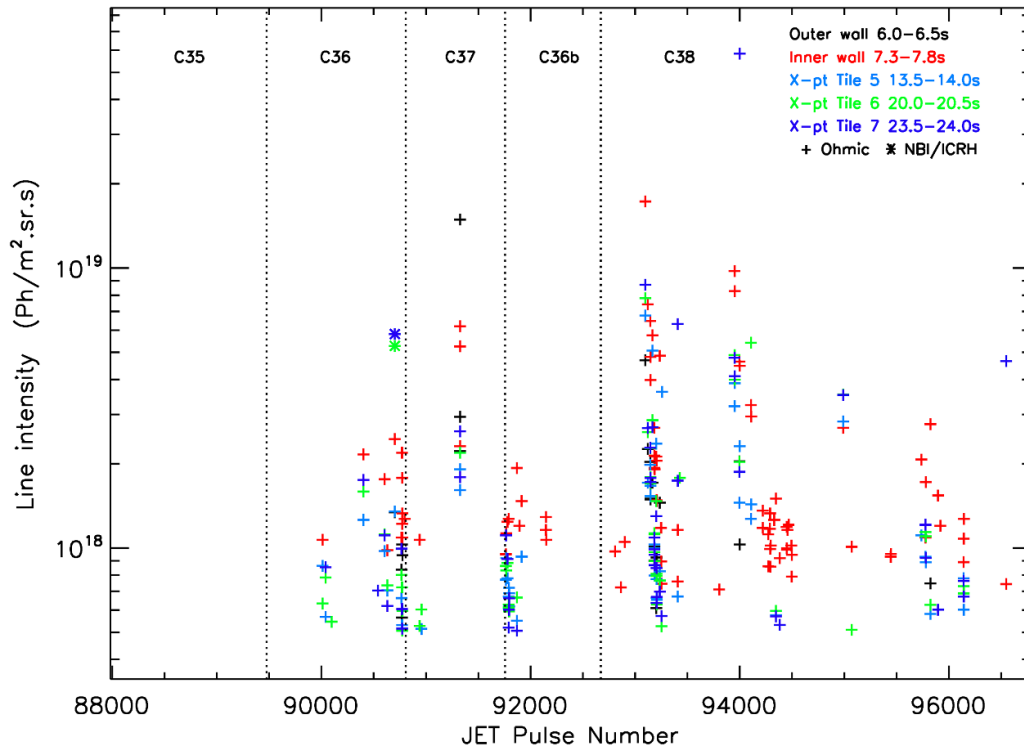
Figure 7. Lyman-α line intensities of He at 303.78 Å observed by KT2.
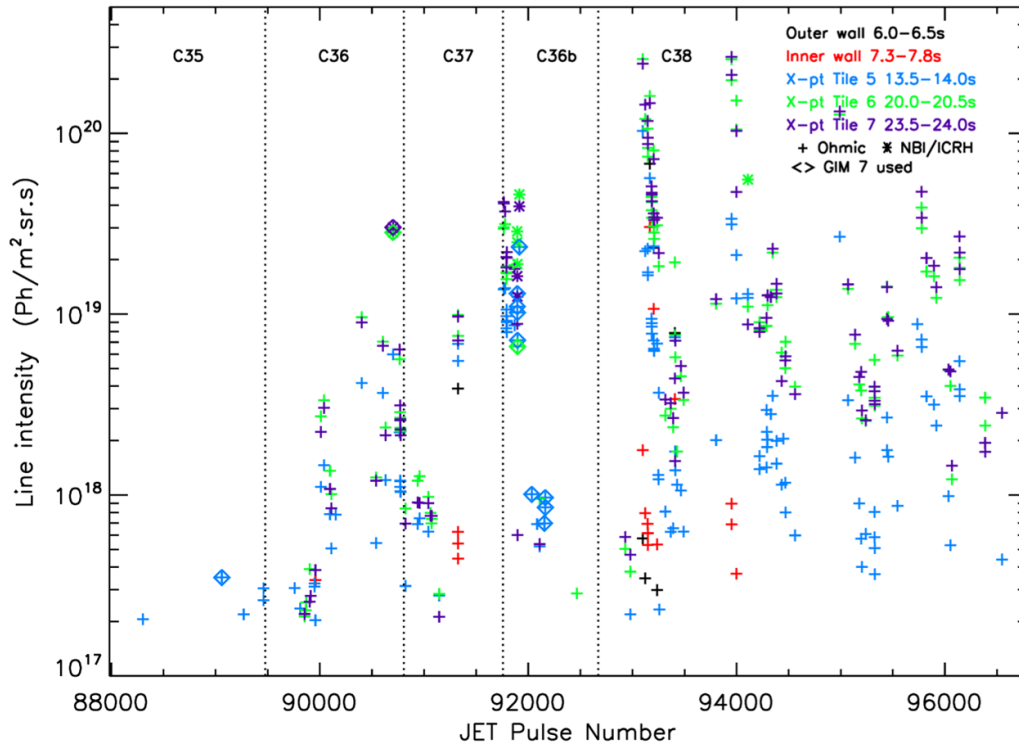
Figure 8. Lyman-α line intensities of He at 303.78 Å observed by KT7/2.

pulses 93023–93089 and 93847–93908 in which He was used as the fuel.

Being a recycling gas with an ionization potential low compared with the other impurity ions considered here, the He emission is strongly dependent on the line-of-sight. This is seen from the differences between the KT2 and KT7/2 signals, with about two orders of magnitude variation in the KT2 line intensity, but with a larger variation of three orders in the KT7/2 intensity. Most observations in the KT7/2 line-of-sight occur during the X-point phases, with those recorded with the outer strike point on tile 6 and tile 7 tending to be higher than those on tile 5. This distinction between the different X-point phases is less obvious with the KT2, horizontal line-of-sight observations. In these the inner wall data is most significant, with very few outer wall points.

3.2. Beryllium

The Be IV (Be^{3+}), Balmer-α line is measured by both KT2 and KT7/2 and is shown for the latter in figure 9. Be is the low-Z element from which the main chamber plasma facing surfaces are manufactured and Be IV the highest ionization stage of Be that can result in line radiation. As already noted, its emission during the limiter phase of a discharge is reproducible to the extent that it can allow a check to be made on the stability of the sensitivity of the recording instrument. This is evident in that the Be signal when the plasma is positioned on the outer and inner walls is approximately constant and confirms the stability of the instrumental sensitivities.

The signals recorded during the X-point phase of the pulse tend to be lower than those of the limiter phases, with the

majority of KT2 observations having additional heating, as is the case for the most intense KT7/2 observations. A few inner wall points in figure 9 are found to have exceptionally high intensities. This is due to the gas injection module (GIM) 7 being used during the measurement. This GIM is sited at the top of the machine on Octant 6 of the torus close to the KT7/2 line-of-sight. The corresponding KT2 measurements made along a horizontal line-of-sight are not exceptional. In the figures diamonds are used to denote KT7/2 measurements recorded when GIM 7 was being used.

3.3. Carbon

C has been observed in JET from the beginning of JET-ILW, although at significantly lower levels than was the case during the JET-C campaigns (Brezinsek *et al* 2013). The lines used to monitor C are the C III line at 977.02 Å, which is observed by KT2, and the C IV line at 312.43 Å, observed by both the KT2 and KT7/2 spectrometers. The C III emission is illustrated in figure 10 and the C IV intensities recorded by KT7/2 in figure 11. Both of these ionization stages occur in the plasma SOL and differences that are due to the horizontal and vertical lines-of-sight of KT2 and KT7/2, respectively, are evident. During the wall phases, the inner and outer wall emission is inverted with the inner wall observations being higher in the horizontal view, the outer wall higher in the vertical view. A difference is also seen in the ordering of the X-point phase intensities. In the vertical view the tile 6 intensities are highest, with either the tile 7 and 5 intensities overlaying, or in the C38 campaign tile 7 exceeding the tile 5 intensities. In the horizontal view the tile 5 emission is highest, with tile 6 and 7
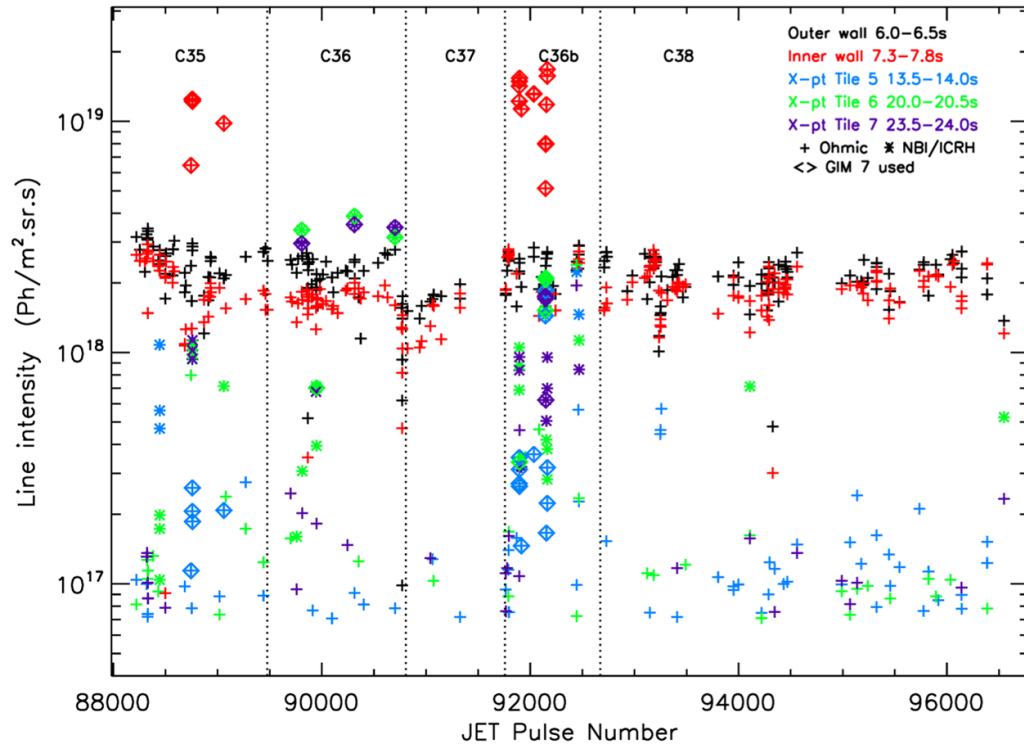
Figure 9. Balmer-α line intensities of Be at 410.06 Å observed by KT7/2.
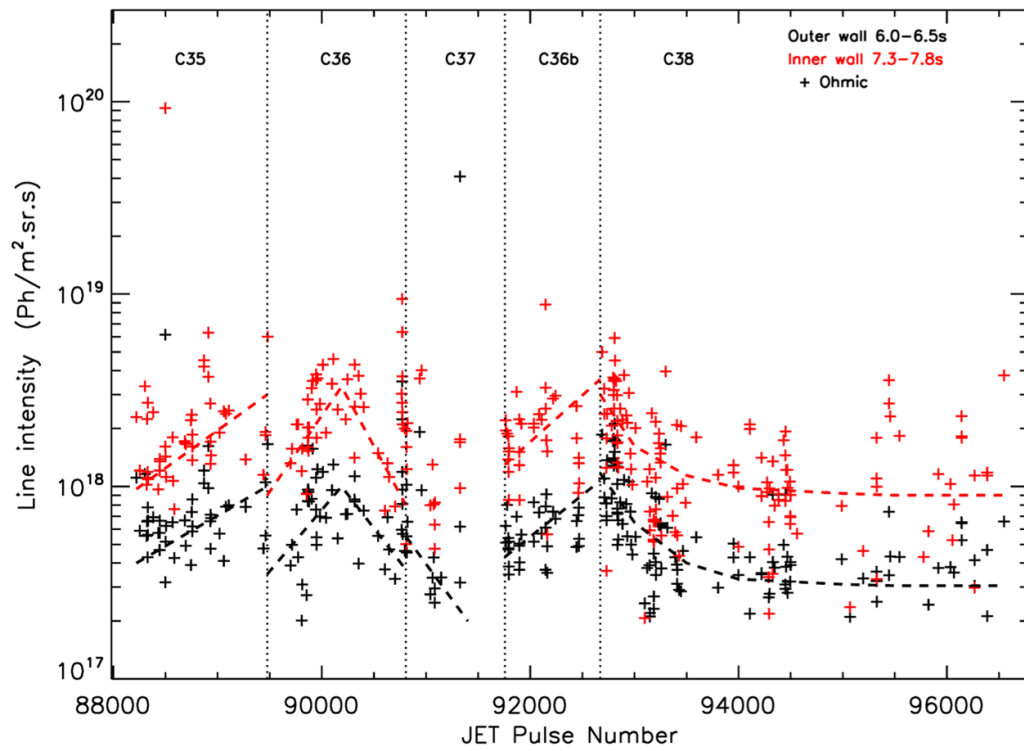
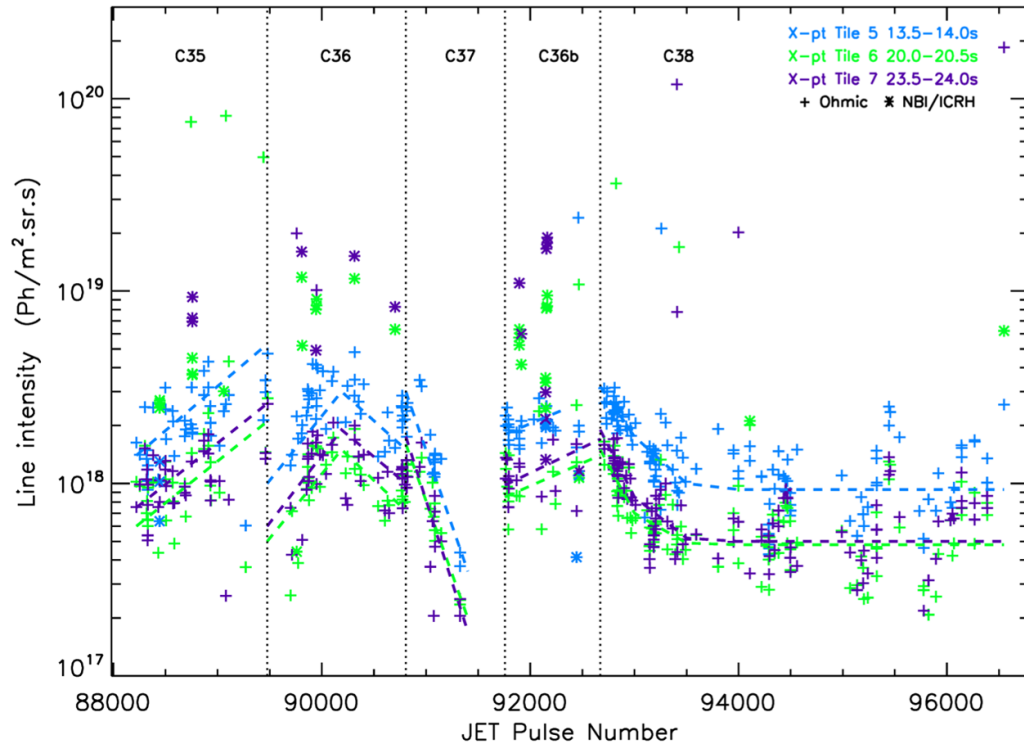**Figure 10a.** Outer and inner wall C III line intensities at 977.02 Å observed by KT2.

Figure 10b. X-point C III line intensities at 977.02 Å observed by KT2.
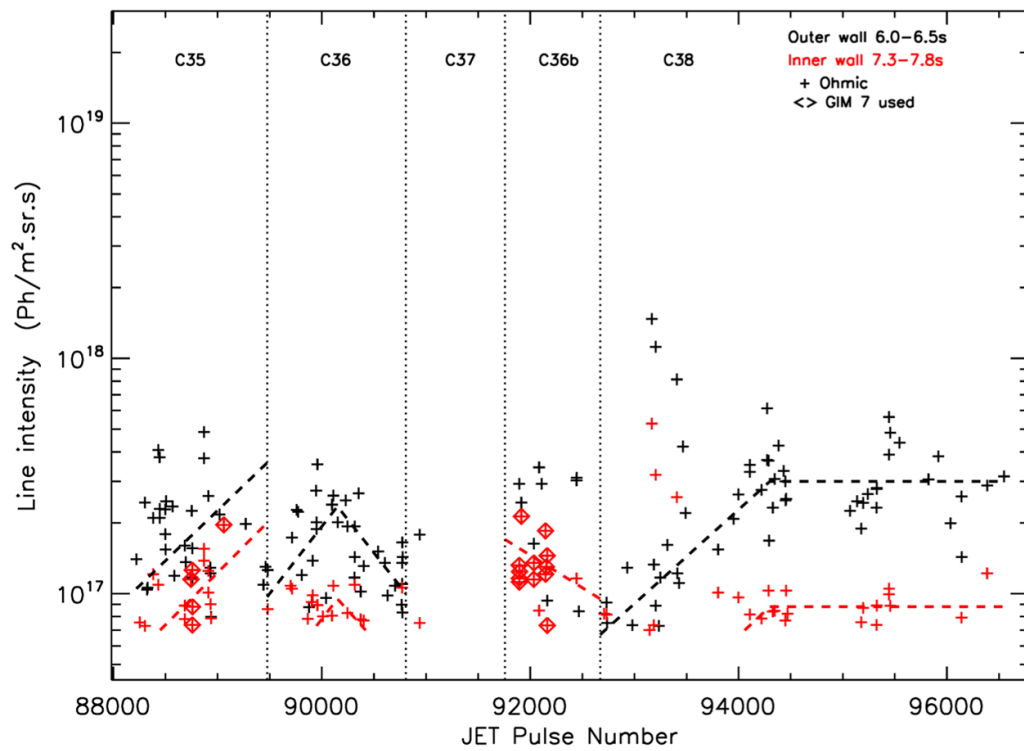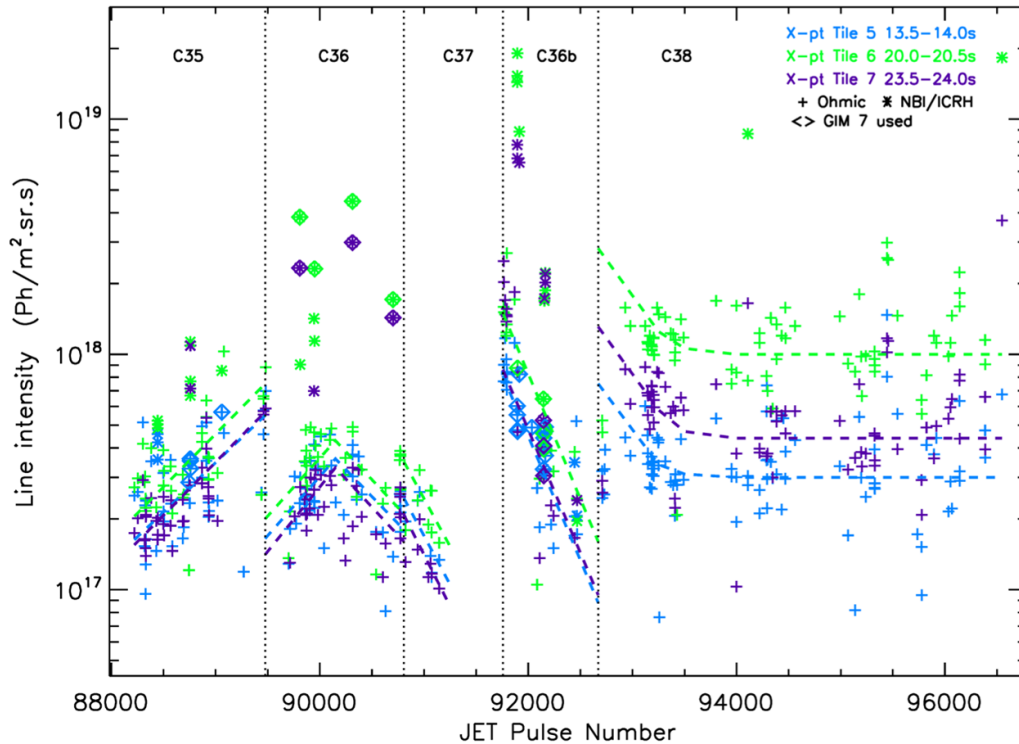

Figure 11a. Outer and inner wall C IV line intensities at 312.43 Å observed by KT7/2.

Figure 11b. X-point C IV line intensities at 312.43 Å observed by KT7/2.

tending to overlay. Lower C levels are seen during the C37 H campaign. In general, similar trends are seen in all the data for a particular element, although two exceptions are noted for C. At the beginning of C38, higher levels that decay to a steadier background level are seen in all observations except the KT7/2 C IV wall data, for which the intensities are initially low then rising to a steadier background level. Further, the KT7/2 C36b and C38 X-point signals are higher than earlier campaigns, with a particularly sharp fall-off in C36b. In the KT2 horizontal view, the C38 observations tend to be lower than in earlier campaigns. It is noted that for C38 this might in part be due to the change in the line-of-sight of the KT7/2 spectrometer. Nevertheless, it should be stressed that no unambiguous evidence has been found that the DiMPle measurements are affected by the change in the KT7 line-of-sight between campaigns C36b and C38.

3.4. Nitrogen

The N IV multiplet at 923 Å is used to monitor this element, which is important in radiative divertor experiments. Increased N levels, which rapidly decay, are seen after its use (figure 12), although there does not appear to be any bias towards a particular surface retaining N more than the others.

3.5. Oxygen

O is routinely seen in the JET plasma and originates in the inevitable small vacuum leaks. Although wall conditioning is better in a metallic machine, Be does retain O in the vessel more so than C, since the Be oxides are less volatile than C

oxides. In pulses 89708–89711 an O seeding experiment was carried out in which O_2 was intentionally gas-puffed. This did not lead to any long term change in the O levels.

O is monitored using the 629.73 Å O V line observed by KT2 and the O V/O VI blend at 173 Å by KT7/2; the former is shown in figure 13. A number of similarities with the C emission are seen. The inner and outer wall emissions are inverted between the horizontal and vertical lines-of-sight and the ordering of the X-point emissions is the same. Lower levels are evident during the C37 H campaign, as well as high initial levels decaying to a more constant background level at the beginning of C38. However, O takes longer to reach a background level than C, $\sim$2500 pulses compared with $\sim$1500 for C. This would be consistent with the O atoms being chemically and therefore more strongly bound to Be than those of C. A difference is also seen in the number of pulses required for the O intensities to decay by 1/e. This is comparatively short for the X-point data, $\sim$425 pulses, but longer for the wall intensities, $\sim$1000 pulses in the case of the outer wall data and $\sim$1800 for the inner wall intensities. The decay times will depend on a number of factors including the cleaning efficiency of the plasma pulses, the bonding and the quantity of O retained on the surface.

3.6. Neon

Ne is monitored using the Ne VIII, 780.32 Å line observed by KT2 (figure 14). Throughout much of the period being studied Ne behaves in a similar way to N being observed immediately after its use in the vessel with no particular bias towards a particular surface. However, a change is seen in the Ne
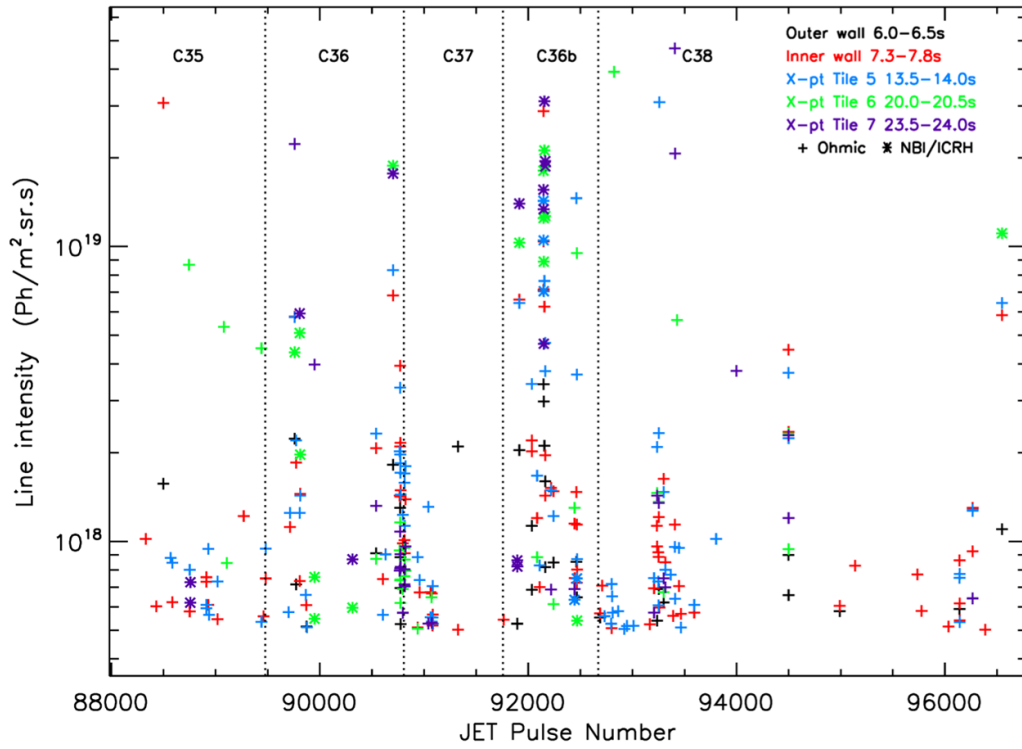
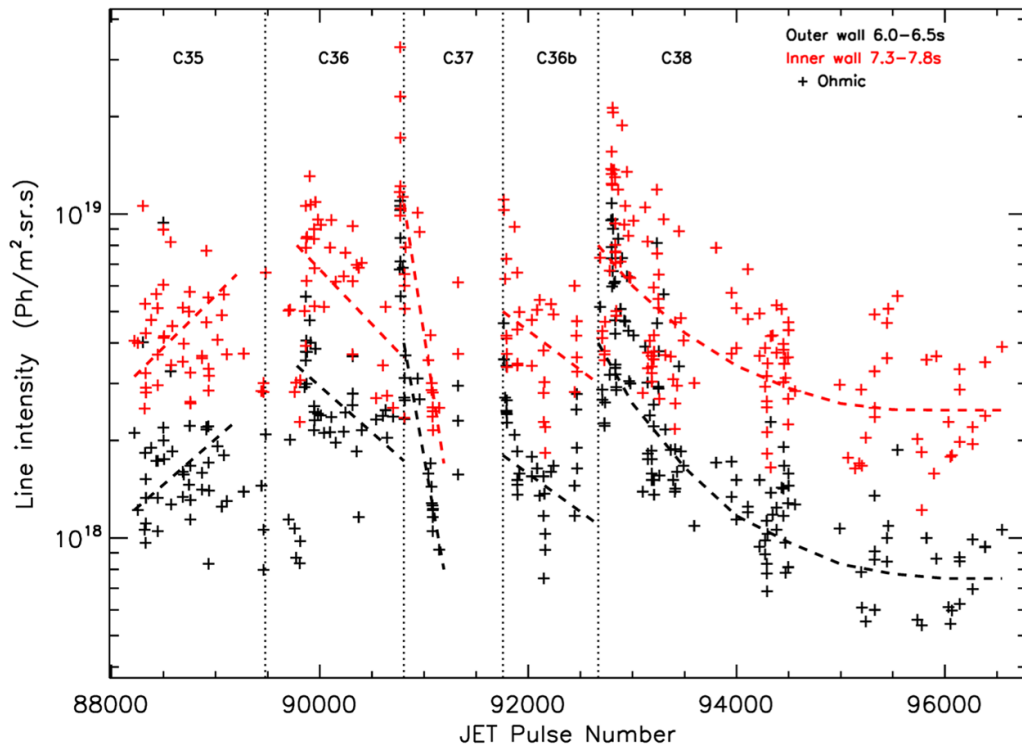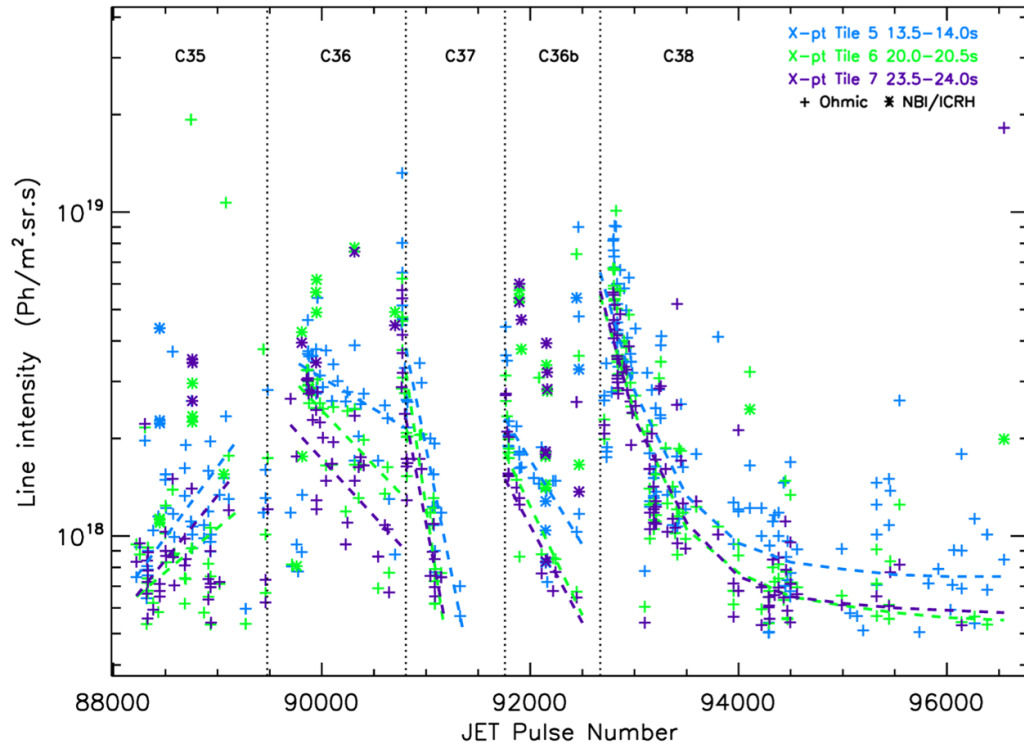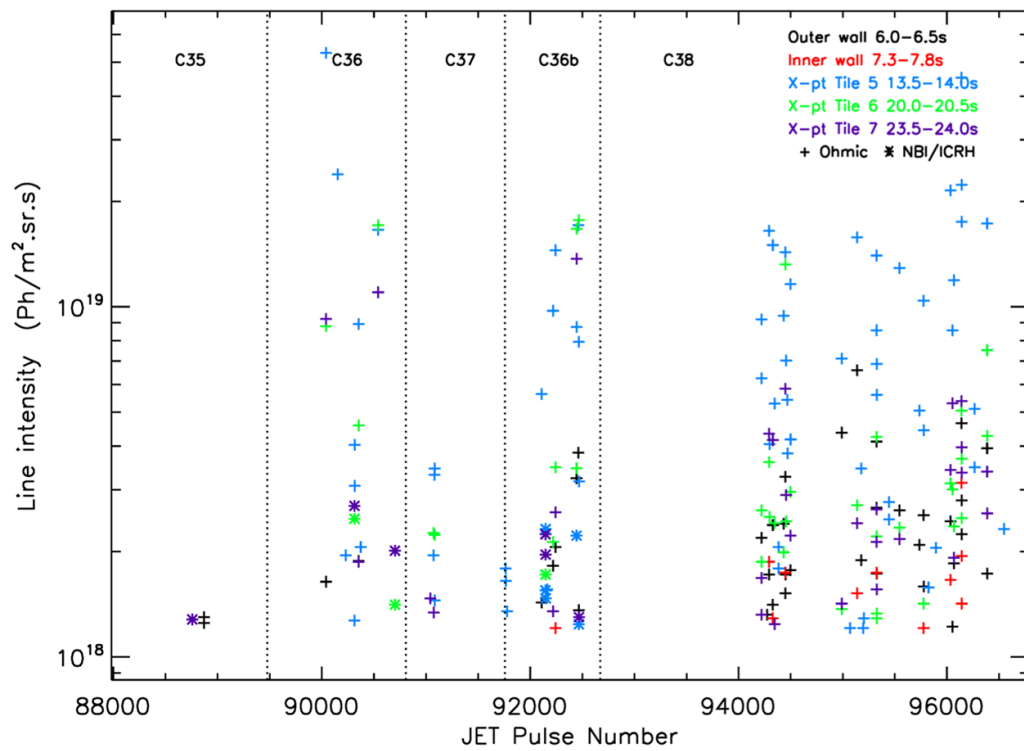**Figure 12.** N IV line intensities at 923 Å observed by KT2.

Figure 13a. Outer and inner wall O V line intensities at 629.73 Å observed by KT2.

behaviour during the C38 campaign after pulse ∼94200. Its use for charge exchange ion temperature measurements has become so frequent that Ne, like Ni and to a lesser extent Cu, has become a feature of the background spectrum, being

routinely observed. This is evident as more frequent observations of Ne in the DiMPle pulses than in previous campaigns and its presence in the spectrum affects the Cl XV measurement. Rather than being distributed around the torus as would

Figure 13b. X-point O V line intensities at 629.73 Å observed by KT2.

Figure 14. Ne VIII line intensities at 780.32 Å observed by KT2.
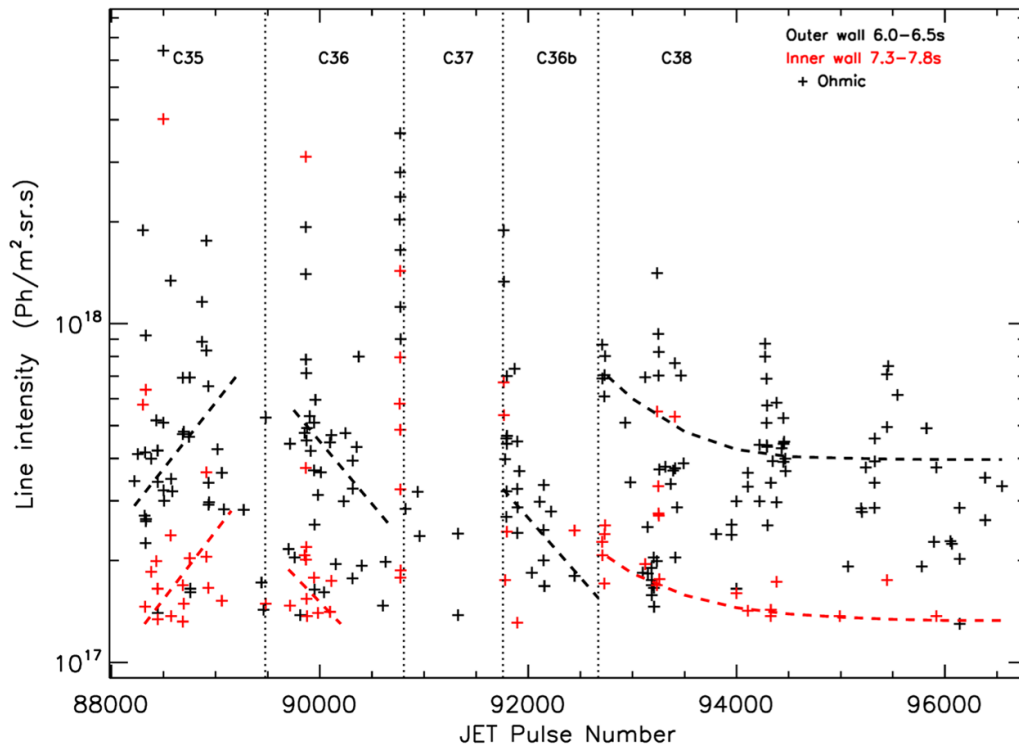
Figure 15a. Outer and inner wall Cl XIV line intensities at 237.70 Å observed by KT7/2.

be expected of any gas during the experiments in which it is used and then rapidly cleaned, it has become embedded in the plasma facing surfaces and is constantly being released. During this later period a tendency for the highest Ne levels to occur during the tile 5 X-point phase of the discharge is seen.

3.7. Chlorine

Of the six intense VUV lines characteristic of mid-Z elements three Cl lines can be seen with a reasonable intensity, although all are blended in the KT2 spectrum. Consequently, it is essential to use KT7/2 to monitor Cl, in which the 237.70 and 415.50 Å lines are resolved. Nevertheless, an additional problem has arisen during C38 with Ne being used so often in JET that Ne lines now form part of the background spectrum. A blend of the Cl XV 415.50 Å line with a Ne V line at 416.21 Å has made the former less reliable. The DiMPle emissions for the Cl XIV 237.70 and Cl XV 415.50 Å lines are shown in figures 15 and 16, respectively.

Cl has been observed in JET from the beginning of the first JET-ILW campaign. It is usually most intense at the beginning of a campaign, probably diffusing to the surface of the plasma facing surfaces during the previous shutdown. Two particularly high excursions are also noted in C36, after pulse 89828 and at the end of this campaign after pulse 90761. In both cases these followed short breaks in operations. The initial cleaning of the surfaces is seen as rapidly decaying spikes, after which a slower decay may be observed. An example of this occurs at the beginning of C38, where the 1/e decay during the X-point phases is ∼900 pulses with there being ∼3300 pulses before a steady background level is reached. That this is longer than

O or C is due to the chemical reactivity of Cl, which makes it more difficult to remove Cl from the vessel. The ordering of the intensities is as for C and O when these are viewed along the vertical line-of-sight.

3.8. Argon

Although the chemical properties of Ar are very different from those of Cl, it has a similar Z and temperature dependence. Again, three intense characteristic lines are observed in the VUV spectrum, that at 353.85 Å due to Ar XVI falling in a relatively clear part of the spectrum. This allows it to be reliably observed in both the KT2 and KT7/2 spectra. The KT7/2 intensities are shown in figure 17 and are very similar to the KT2 observations of this line (Lawson and Coffey 2020). Unlike the lines for the low-Z elements, which are emitted from or close to the SOL, Ar XVI is emitted from the plasma core and the similarity of the KT2 and KT7/2 observations demonstrates that the lines-of-sight of the spectrometers do not affect the results for this ion. Although it was not possible to confirm this for Cl, the same conclusion is expected to apply to the lines used to monitor Cl. The observations for the 221.15 Å, Ar XV line are also found to be very similar to those in figure 17. This shows that this line is a reliable monitor of Ar, despite the spectral region around 200 Å being crowded.

The highest intensities of Ar follow its previous use immediately before the observations, either in experiments or injected through the disruption mitigation valves (DMVs). As with He and N a rapid decay of the emission follows, although to more substantial backgrounds than for the lighter gases. The spikes in intensities are comparable to those seen for Cl,
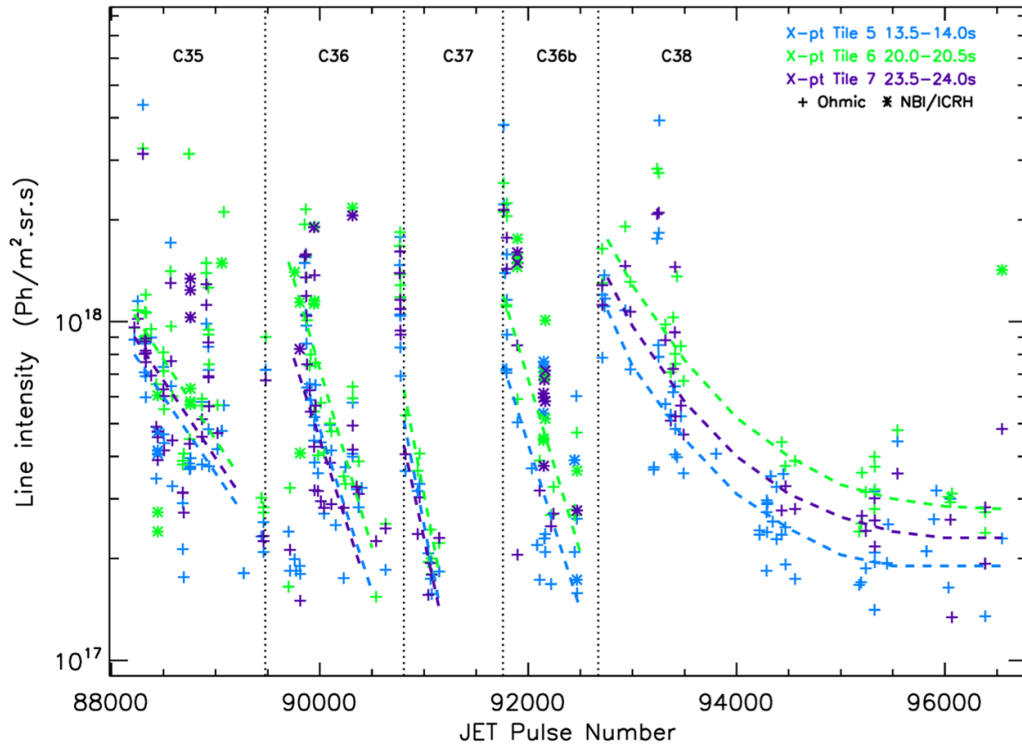
Figure 15b. X-point Cl XIV line intensities at 237.70 Å observed by KT7/2.
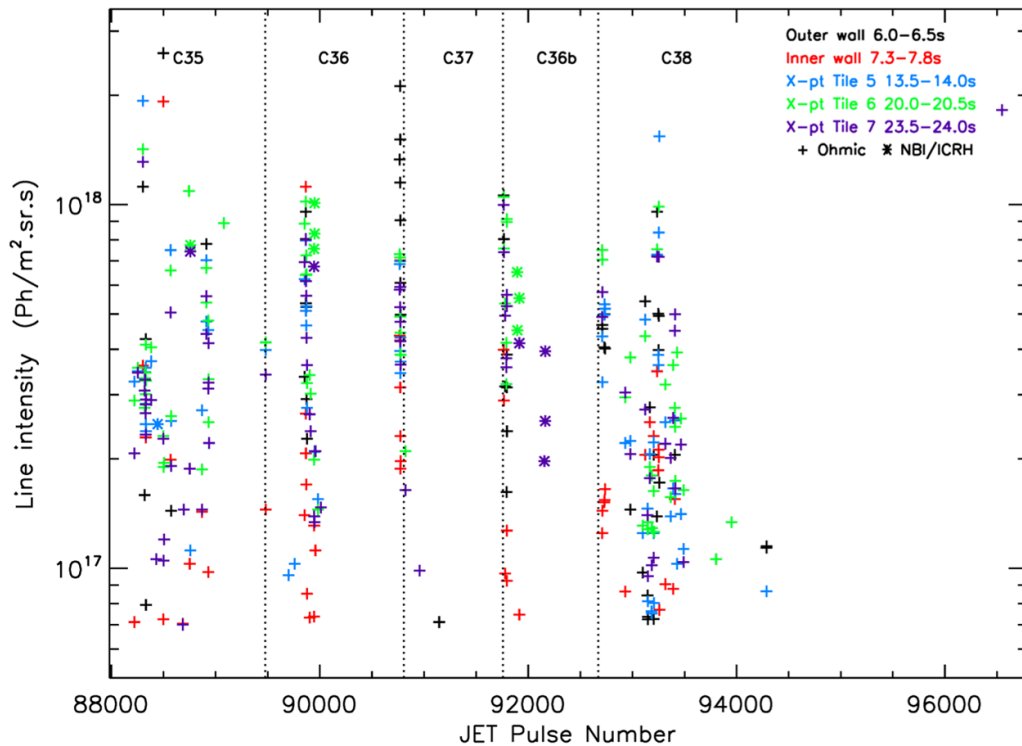

Figure 16. Cl XV line intensities at 415.50 Å observed by KT7/2.

although they are not followed by the slower decay phase observed for Cl. The chemical reactivity of Cl means that it is less easily removed from the plasma facing surfaces than Ar. Nevertheless, there is a similarity in that in both sets of data there is a tendency for the emission during the outer wall phase to be higher than the inner wall phase. However, during the X-point phases, the Ar emission when the X-point is positioned on tile 5 tends to be higher than that for tile 6 and 7, which
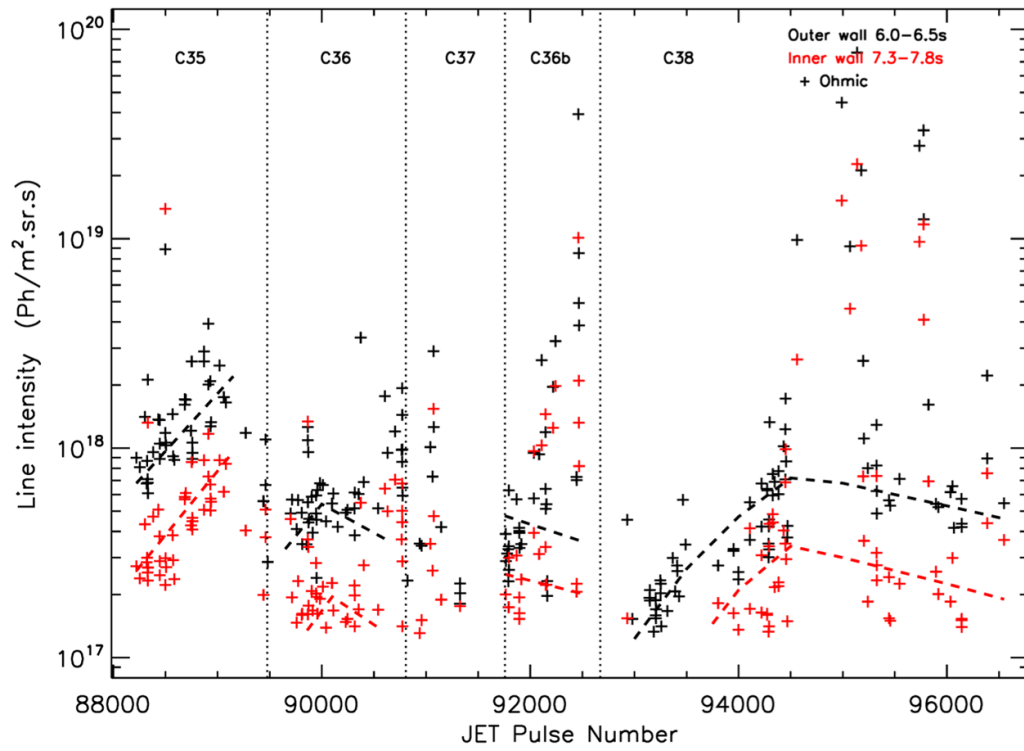
Figure 17a. Outer and inner wall Ar XVI line intensities at 353.85 Å observed by KT7/2.

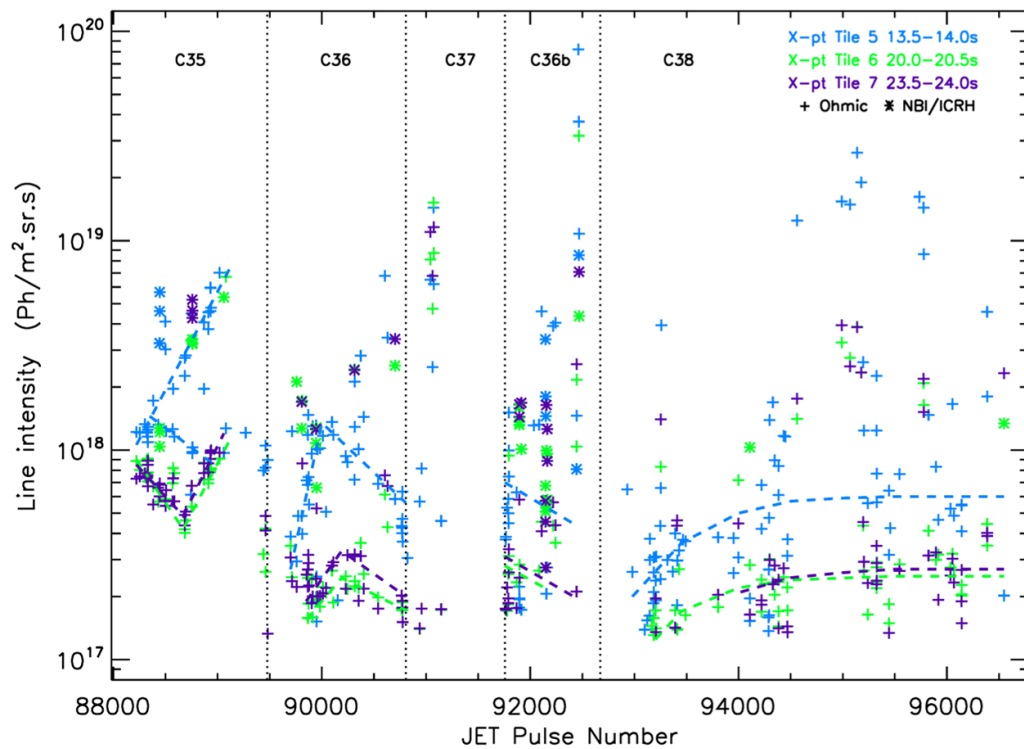**Figure 17b.** X-point Ar XVI line intensities at 353.85 Å observed by KT7/2.

largely overlay. This contrasts with the observations for Cl for which the tile 5 emission is the lowest. Again, this is expected to be due to a difference in the deposition and the release and cleaning mechanisms expected for these chemically very different gases. The ease with which the tile 5 surface is cleaned of Ar during a discharge will lead to a higher contamination of the cleaning plasma.

3.9. Titanium

The source of the recently observed Ti influxes has been identified as a coil in the upper part of the JET vessel between Octants 3 and 4. Through ageing the material is becoming unstable possibly through oxidation, although there is no evidence of O or any other element entering the plasma at the time of the influxes, the influxes being pure Ti. Influxes are seen in 8 C35 to C36b DiMPle pulses and three pulses towards the end of C36b and two in C38 show background levels of Ti rather than sharp influxes.

As with Cl and Ar there are three characteristic lines that are useful in monitoring Ti, the Ti XIX line at 169.58 Å and a Ti XX line at 259.29 Å being used. Since this spectral region has numerous lines, a condition that both Ti lines are observed and that the lines are significantly more intense than a neighbouring W line is imposed to ensure that the observations are a reliable monitor of this element.

3.10. Mid-Z elements—chromium, iron, nickel and copper

Of the six intense lines that characterize the VUV spectrum of many elements, the Be- and Li-like lines have been used for Cl, Ar and Ti. For the mid-Z metals Cr, Fe, Ni and Cu the Mg- and Na-like lines better match the temperature of the emitting plasma. This is because the DiMPle pulses are either Ohmic or have only modest heating powers with the result that it is these lower temperature lines that are observed with high intensity. The stronger line of the Na-like doublet observed by the KT7/2 spectrometer has been used to monitor these elements (table 2), observations of this line by KT2 also being studied for Ni and Cu. The use of the same transition has allowed a direct comparison to be made between these elements. In the case of Cr there is concern about blending of the Na-like line with Ar and, consequently, data for the Mg-like Cr transition at 328.27 Å has been included in the study. The similarity between the two Cr datasets confirms that the Na-like line is a reliable monitor providing pulses in which Ar is significant are excluded. The KT2 and KT7/2 data for both Ni and Cu are similar, confirming that the line-of-sight does not affect the emission from these core lines.

Both Cr and Ni originate in the Inconel from which the JET vessel is constructed. Ni is the most persistent of the background elements and is almost always seen in the VUV spectrum to a lesser or greater extent. In most discharges, Cr is only seen weakly, its observation exacerbated by blending of its characteristic lines. Fe has long been a background element in JET, resulting in occasional strong influxes. One of the original sources of Fe was the lower hybrid current

drive launcher, which was decommissioned at the end of the C34 campaign in October 2014; other sources present in the machine include the stainless steel LIDAR beam dump. Like Ni, Cu is seen routinely in JET, at times exceeding the emission due to Ni. Its main source is the NBI ducts, although, in the past, it has also been released from earlier ICRH antennas.

The behaviour of the mid-Z elements is illustrated in figures 18 and 19, which show the KT7/2 observations of the Fe XVI and Cu XIX intensities. The outer wall limiter intensities are found to be higher than those during the inner wall phase for a number of elements and for the mid-Z elements this difference is very significant being close to an order of magnitude. The X-point intensities lie closer to each other, with those when the outer strike point falls on tile 6 being the highest, on tile 5 the lowest. The intensities rapidly decay when H is used as fuel in campaign C37 and all elements also show lower levels rising to a steadier background level at the beginning of the C38 campaign. It is noted that the X-point data becomes progressively smaller relative to the limiter data with increasing Z. The Cr X-point data overlays the higher outer wall data whereas for Cu the X-point data overlays the inner wall emission. The dependence on Z is thought coincidental and this behaviour more likely reflects the material properties and the ease of release of the different elements.

3.11. Krypton

During the earlier campaigns covered by the present study Kr was used as a DMV gas in JET. Only eight DiMPle pulses show significant Kr, this appearing immediately after its use. It is monitored using the 178.99 Å, Kr XXVI line. Since there are numerous W lines in this spectral region, the Kr XXVI line is required to be significantly more intense than two neighbouring lines that are due to W.

3.12. Molybdenum

Mo was first observed in JET plasmas in the C31 campaign, being seen in a low temperature, post-disruption spectrum of pulse 84747, in which Mo V to Mo VII features were identified. At this time, it is thought to have come from the Mo substrate of W coated tiles in the outer corner of the JET divertor. It is also found on the back panels of the NBI calorimeters, which in more recent campaigns has led to Mo entering the torus when NBI is used. In C38 a number of Mo influxes from the neutral beams led to disruptions.

Mo is monitored using the two Na-like Mo XXXII lines at 127.87 and 176.65 Å. The latter is observed by KT7/2, but because of the numerous W lines in this region has proved to be a relatively insensitive monitor of this element. The 127.87 Å line is preferred and its intensity is shown in figure 20, although this line is also affected by blending. The limiter data for Mo are mainly from the outer wall phase, with nearly all the X-point data occurring during additional heating. Nevertheless, despite the rather limited data available, the tile 6, tile 7, tile 5 ordering is evident.
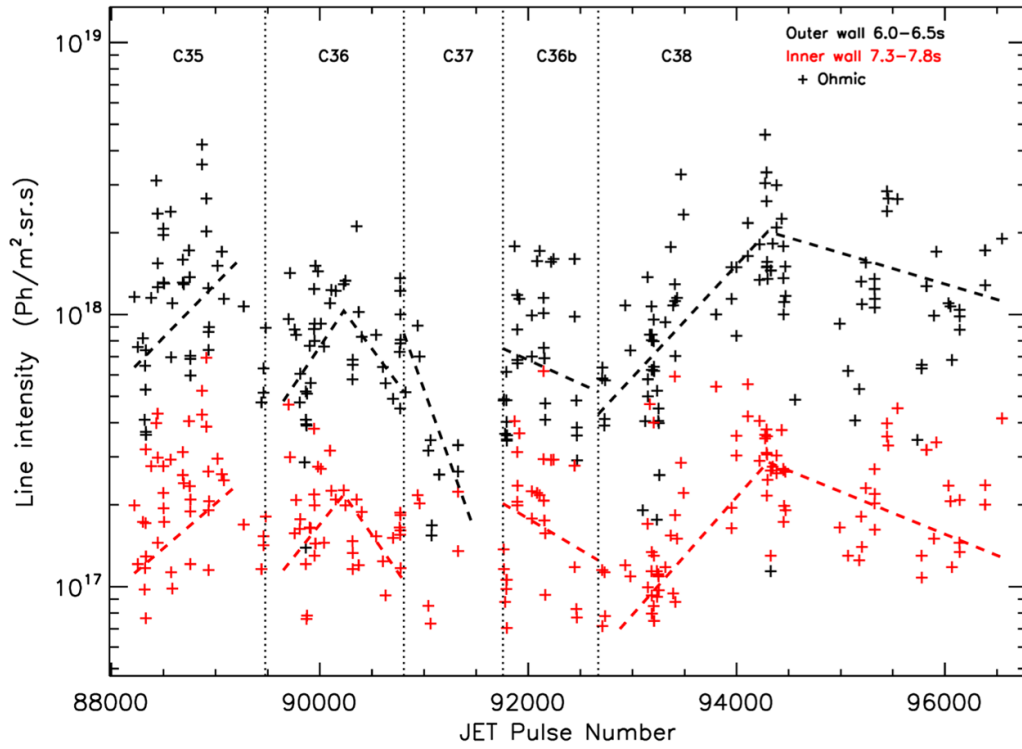
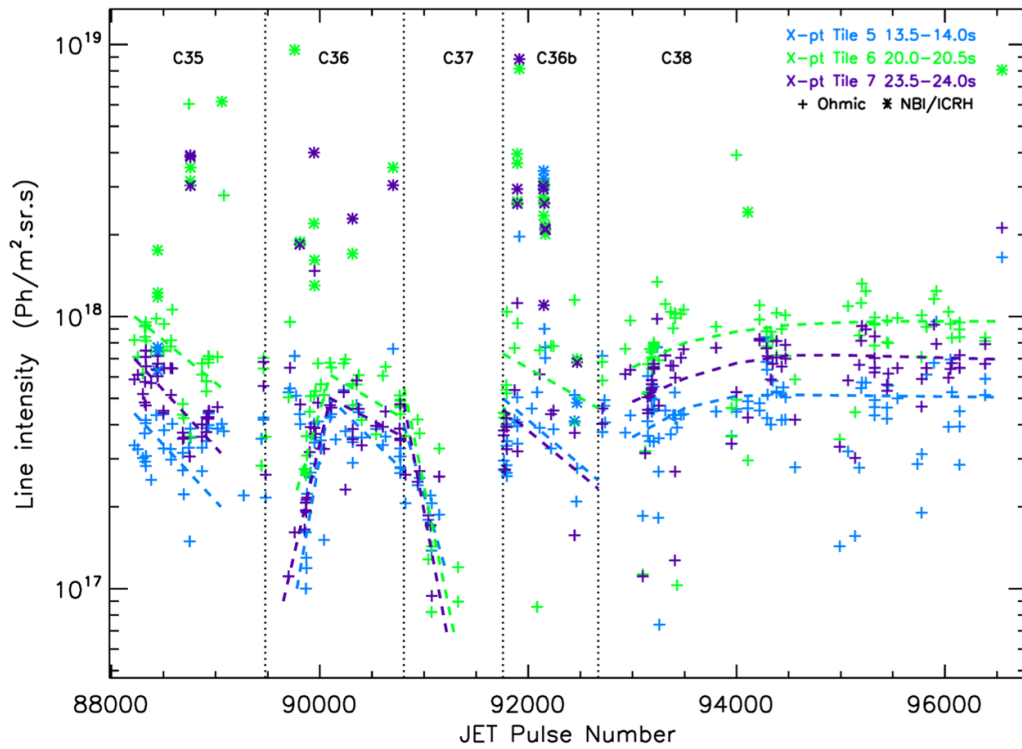**Figure 18a.** Outer and inner wall Fe XVI line intensities at 335.41 Å observed by KT7/2.

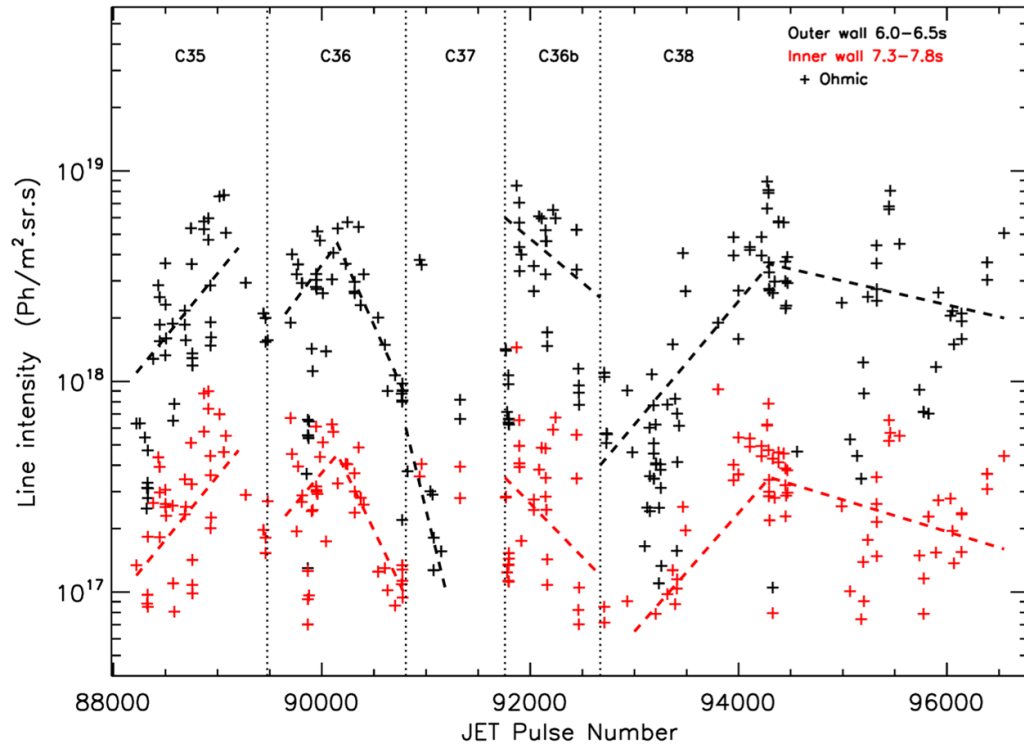**Figure 18b.** X-point Fe XVI line intensities at 335.41 Å observed by KT7/2.

Figure 19a. Outer and inner wall Cu XIX line intensities at 273.35 Å observed by KT7/2.

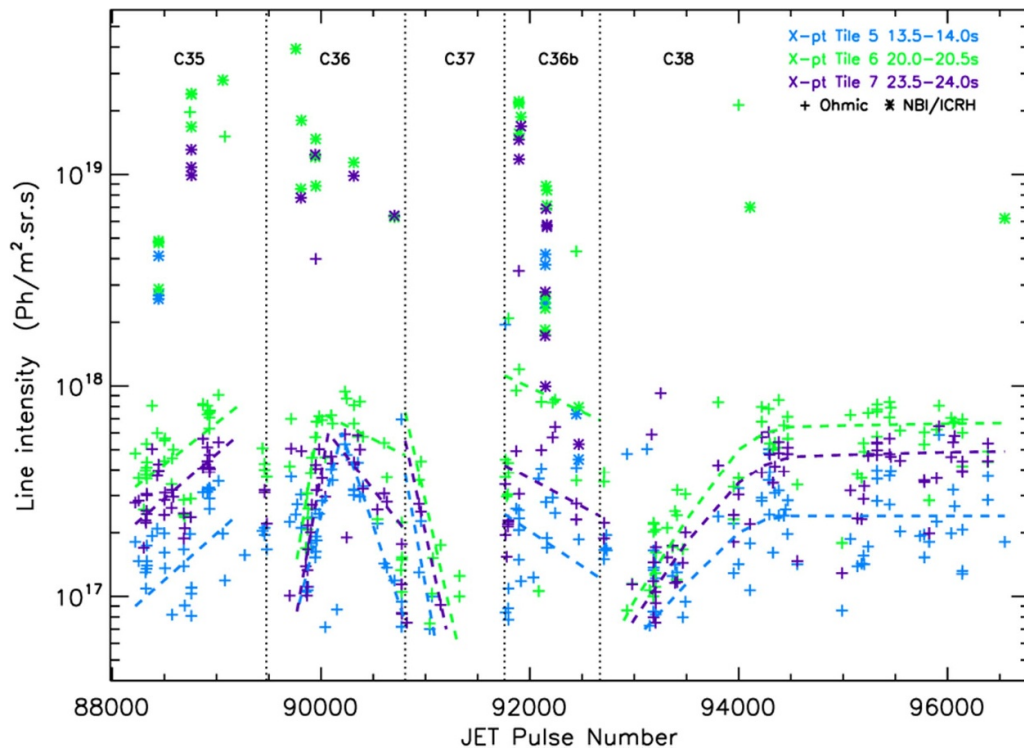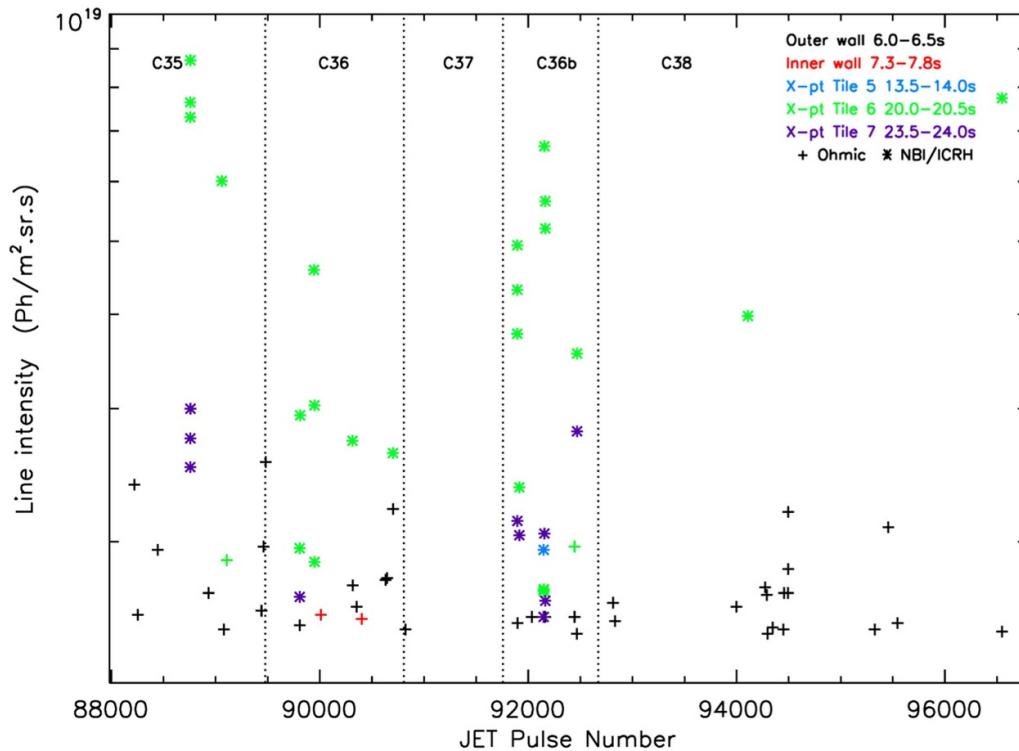**Figure 19b.** X-point Cu XIX line intensities at 273.35 Å observed by KT7/2.

Figure 20. Mo XXXII line intensities at 127.87 Å observed by KT2.

3.13. Tungsten

Three measurements of W have been studied, two involving the UTAs observed in the KT2 spectrum and the third those in the KT7/3 spectrum. The first of these is the usual KT2 W feature in which the KT2 spectrum is integrated from 147 to 213 Å. Its limitation is that it includes lines from a number of other elements, some of which can be intense. An improved measure (WIK) designed to exclude, as much as possible, the contaminating features was developed and being most sensitive is shown in figure 21. The third measure integrates the UTAs from 42 to 54 Å in the KT7/3 spectrum. With the available, rather limited data no significant difference is found between the KT2 and KT7/3 results. The behaviour of the W is similar to that of Mo.

4. Discussion

4.1. Behaviour of gaseous impurities

The impurities observed in the JET plasmas can be divided into two groups, although with some overlap. The first group contains the gases that are introduced into the torus for particular experiments by puffing, He, N, Ne, Ar and Kr, and the second those released into the plasma from the plasma walls or components within the vessel. These include Be, C, O, Cl, Ti, Cr, Fe, Ni, Cu, Mo and W. The behaviour of the gases is the more straightforward in that high levels of the element are seen immediately after an experiment. There is a rapid decay as the plasma facing surfaces are cleaned with no particular pattern to the behaviour; essentially the gas fills the torus and

the subsequent cleaning depends on the plasma configurations used in the pulses following the gas-puffing experiment. This is illustrated in figure 22, which shows the normalized KT2 intensities as a function of pulse number following the element's first observation in a DiMPle pulse. There are measurements at more than one time in this first pulse and the normalization is made to the geometric mean of these measurements. With this much-expanded pulse number scale it can be seen that there is a significant drop in the N, Ne and Ar intensities within a few pulses. The number of pulses for a 1/e fall in intensity is 5, 4 and 3, respectively, that for Ne being an estimate, since the available data is limited. Subsequently, there are only occasional observations of N and Ne, but at a low level. In the case of Ar, the background levels tend to be higher than for the lighter gases, with a behaviour consistent of Ar being retained in the vessel. The higher concentrations of He in the plasma, particularly when it is used as the fuel, also lead to a greater retention of He on the plasma facing surfaces. This results in a slower decay with a 1/e fall of 19 pulses. Nevertheless, subsequent to the decay phase, there are only occasional observations of He, as is observed for N and Ne.

However, a difference is found if a gas is used extensively in a campaign as, for example, has been the case for Ne during the later part of the C38 campaign. After pulse ∼94200, its use has been so frequent that it is routinely observed, even if only at low levels, frequently forming part of the background spectrum. Again, the atoms become embedded in the plasma facing surfaces and then progressively released into the plasma.

Although O falls in the second group of elements being retained on the plasma facing surfaces, there has been one O
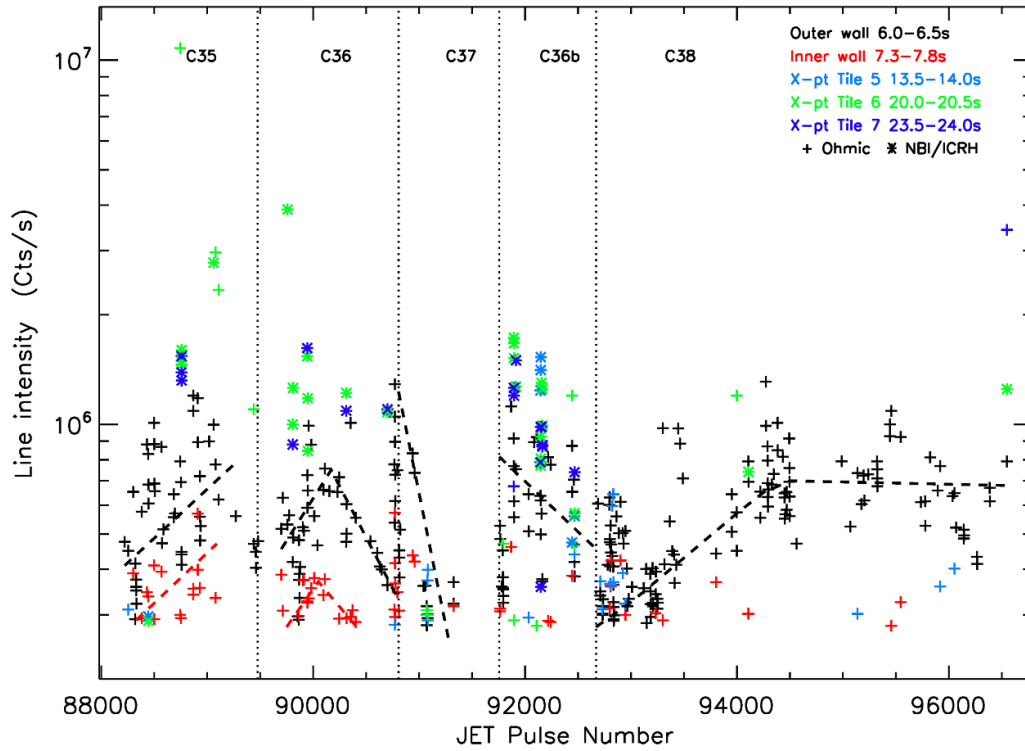
Figure 21. W intensity indicator observed by KT2.
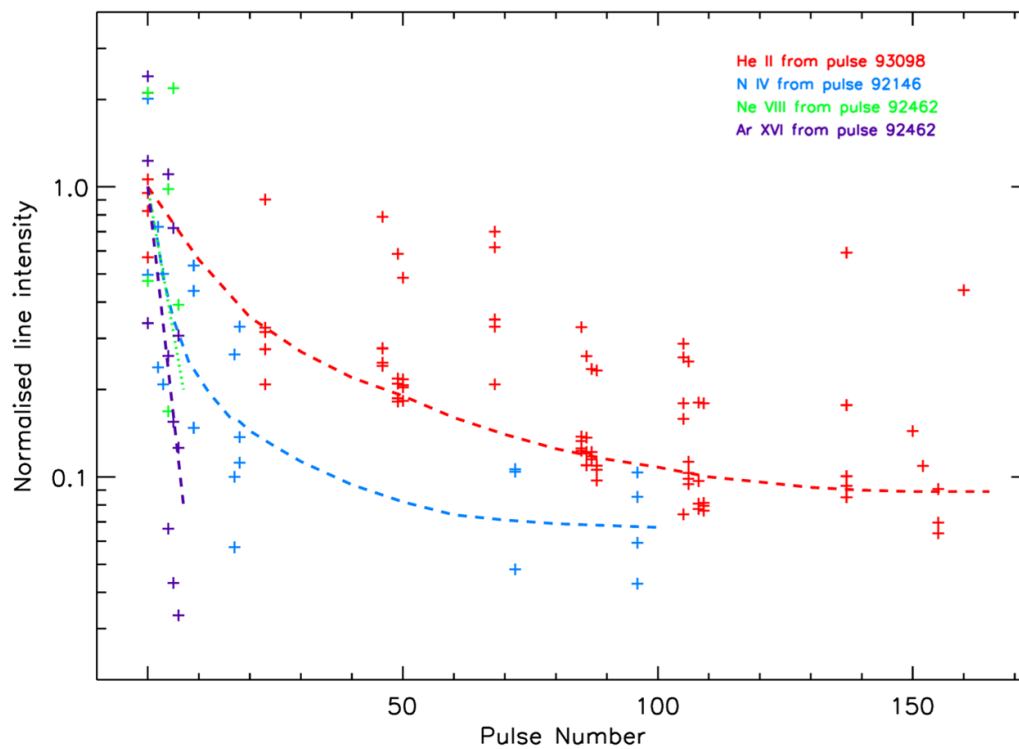
Figure 22. Decay of impurities introduced by gas-puffing.

seeding experiment carried out on JET in which O_2 was gas-puffed (section 3.5). This experiment had little effect on the long-term O levels, which returned to the typical background levels within a few pulses.

4.2. Impurities retained on plasma facing surfaces

In contrast to the gaseous impurities, a systematic behaviour is observed for the second group of impurities retained in the
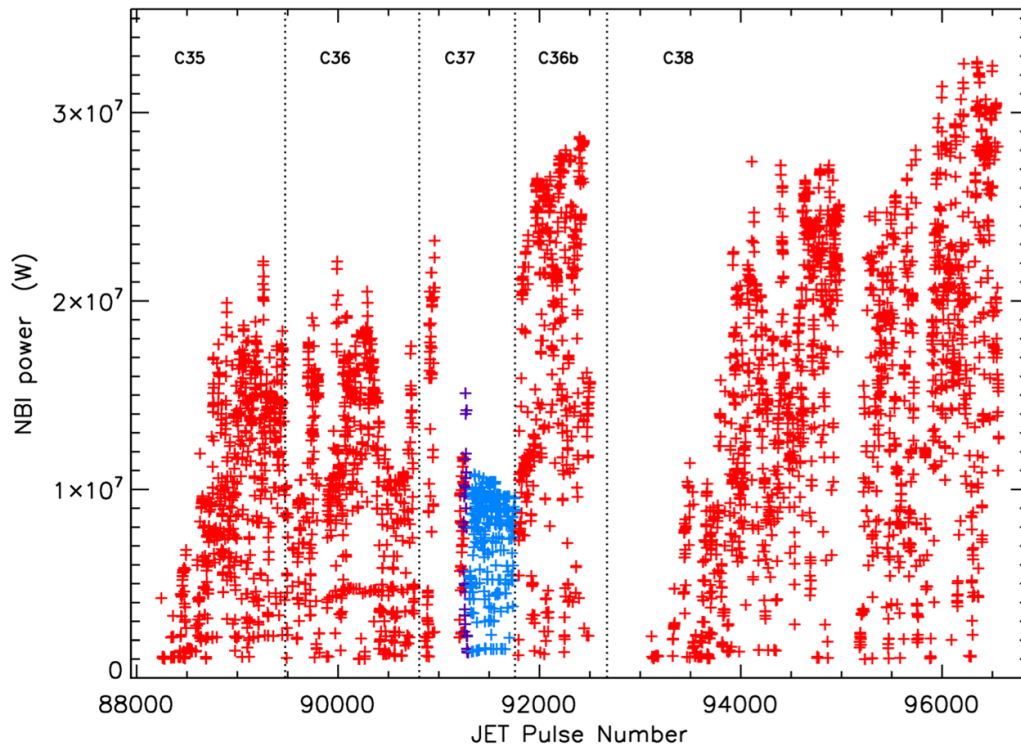
Figure 23. Maximum NBI powers. D beams both octants shown in red, octant 4 H octant 8 D in purple, H beams both octants in blue.

vessel on plasma facing surfaces. The post-mortem analysis of such surfaces in JET are discussed by authors, such as Rubel *et al* (2013) and Ström *et al* (2019). The behaviour depends on a number of factors, including the most frequently used plasma configurations, which will lead both to deposition and to preferential cleaning of certain surfaces, and the precise mechanisms involved in the atoms being retained on the surface. In some cases these involve the formation of chemical complexes or compounds as is expected for Cl and O; in others the retention depends on physical processes. A difference is also noted between filling the torus with a gas when the atoms are adsorbed onto the surface, which can then be readily cleaned, and running a plasma discharge from which ions are emitted with enough energy to be embedded in the surface, this particularly so if the plasma terminates in a disruption. As seen with Ne in the latter part of C38, the more frequently the impurity occurs in the plasma the more of it is absorbed and to a greater depth either by direct impact or diffusion. Subsequently, a plasma will tend to clean the surface removing impurities from it, although this contaminating the cleaning plasma.

4.3. Impurity influxes due to dust particles

All the elements in the second group apart from O and Cl are solids. Solids can also enter the plasma in the form of dust (Uccello *et al* 2016). Such events are characterized by sharp influxes, which have no spectroscopic precursor (Sertoli *et al* 2015a, 2015b), but which can present a significant hazard to the operation of large plasma machines (Tolias *et al* 2018). They are observed only at the time of the influx and in this respect are more like the gases that are seen immediately after

their use in the vessel. However, like gases, if the influxes occur frequently, the element can be dispersed around the vessel surfaces and subsequently give rise to a background emission. This was beginning to happen with Ti towards the end of the C36b campaign.

4.4. Impurity levels during H campaign

Elements within the second group are found to have lower impurity levels during the C37, H campaign mainly due to the reduced physical sputtering of the lighter fuel ions. However, as is shown in figure 23, the NBI powers were also lower during this campaign in part due to the availability of the different beam boxes and also due to the lower powers achieved with H beams; this factor may also play a role.

The lowering of the impurity levels during H operations would lead to the expectation of increased levels during tritium and deuterium-tritium operations. However, from the available data it is not possible to make quantitative predictions for such changes.

4.5. Reduced metallic impurity levels during C38 restart

Reduced levels of the mid-Z metallic elements during the long restart period at the beginning of the C38 campaign, seen particularly clearly during the limiter phases, but also evident in some of the X-point phases, appear mainly due to the higher C, O and Cl levels at this time limiting the transport of the metals into the core plasma. With the available data, an anti-correlation of the metal and C, O and Cl levels is best illustrated by the outer limiter O V and Ni XVIII line intensities
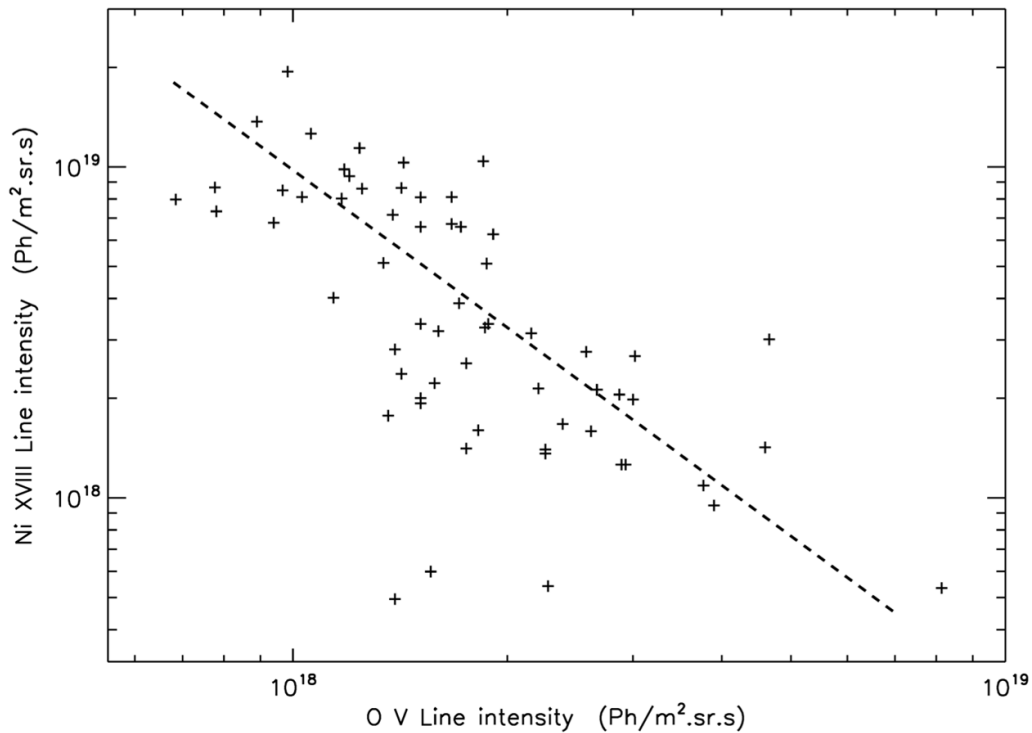
Figure 24. Outer wall O V: Ni XVIII line intensities during the C38 restart period.

shown in figure 24. Similar trends are observed for C and Cl, although with more scatter in the data. In this case the limited NBI powers (figure 23) achieved during this restart period led to a slower cleaning of the plasma facing surfaces than is usual at the beginning of a campaign. Although the lower beam powers might also affect the metal levels, it is seen that a further increase in the NBI powers after pulse 95994 does not lead to a further rise in the metals. Figures 18 and 19 show that the metals reach a steady background level at about the same time as O (figure 13), with C (figure 10) somewhat earlier and Cl (figure 15) later. The metal levels subsequently remain roughly constant or even decay. Figure 21 shows that W is affected in the same way as the mid-Z elements during this period.

4.6. Behaviour of impurities retained on plasma facing surfaces

The complexity of the retention and release of the impurities results in a number of different observed behaviours. As is seen immediately after the use of gases, there can be a sharp fall in the impurity level, followed by a slower decay. This is seen particularly for Cl at the beginning of a campaign; it is supposed that Cl diffuses to the wall or divertor plate surfaces during the period of the shutdown resulting in its ready release in the first discharges of the new campaign. Other elements such as C and O can also show a slow decay as they are cleaned from plasma facing surfaces (for example at the beginning of the C38 campaign) before they reach a steadier background level.

The spectroscopic observation of impurities may be affected by line-of-sight factors. This applies to low-Z elements where the emission originates in the SOL of the plasma and can be enhanced by the local release of an impurity directly into the volume viewed or through SOL flows into this volume. Therefore, to understand which of the plasma facing surfaces gives rise to the highest impurity levels, line intensities of the higher Z elements emitted from the plasma core should be considered first, since these are least likely to be affected by such issues. That this is the case is confirmed by the similarity of the horizontal KT2 and vertical KT7/2 observations for Ar, Ni and Cu. Both KT2 and KT7/2 measurements show that the outer wall emissions are significantly higher than those of the inner wall. Therefore, for the higher Z impurities (confirmed for $Z = 18$, but likely to apply to elements with a similar Z) either the horizontal or vertical measurement will be a good monitor of the plasma impurity level.

For the low-Z elements, the vertical KT7/2 line-of-sight is thought to provide the more reliable monitor of the impurity levels during the limiter, wall phases of the discharge, since this does not directly view a surface from which impurities can be released. Again, this indicates that the outer wall phase has higher impurity levels than the inner wall phase although the difference is less marked than for the higher Z elements. For these elements, the horizontal KT2 view shows a reversal of impurity levels with the inner wall exceeding the outer wall level most likely because the measurement is affected by impurities released from the inner wall into the plasma volume being observed. That this does not happen to the same extent when the plasma is on the outer wall may in part be due to

Table 4. Comparison of mid-Z element intensities recorded with KT7/2 (photons m^{-2} sr^{-1} s^{-1}).

Phase	Pulse range	Cr	Fe	Ni	Cu
Outer wall	88222–90806	7.3e + 17	1.1e + 18	5.6e + 18	2.9e + 18
Outer wall	91757–92671	6.5e + 17	7.2e + 17	5.0e + 18	4.2e + 18
Outer wall	92671–96548	1.1e + 18	2.0e + 18	9.0e + 18	3.6e + 18
Inner wall	88222–90806	1.7e + 17	1.8e + 17	1.3e + 18	3.5e + 17
Inner wall	91757–92671	1.6e + 17	1.5e + 17	1.1e + 18	2.2e + 17
Inner wall	92671–96548	2.0e + 17	2.9e + 17	1.8e + 18	3.5e + 17
X-point—tile 5	88222–90806	3.0e + 17	3.8e + 17	1.3e + 18	2.3e + 17
X-point—tile 5	91757–92671	3.4e + 17	4.1e + 17	1.3e + 18	1.8e + 17
X-point—tile 5	92671–96548	5.5e + 17	4.8e + 17	1.8e + 18	2.5e + 17
X-point—tile 6	88222–90806	6.9e + 17	6.6e + 17	2.8e + 18	6.1e + 17
X-point—tile 6	91757–92671	7.7e + 17	7.0e + 17	3.0e + 18	8.3e + 17
X-point—tile 6	92671–96548	1.0e + 18	9.0e + 17	3.2e + 18	6.2e + 17
X-point—tile 7	88222–90806	4.8e + 17	4.6e + 17	2.0e + 18	4.3e + 17
X-point—tile 7	91757–92671	5.6e + 17	3.6e + 17	1.7e + 18	2.5e + 17
X-point—tile 7	92671–96548	6.0e + 17	7.3e + 17	2.6e + 18	4.4e + 17

the viewing geometry with the line-of-sight passing through a large port away from the site of the impurity release. It will also be affected by differences in the inner and outer wall release mechanisms. In contrast, no difference is seen for Be and this may well be a consequence of this element being monitored by a Be IV line, an ionization stage straddling the last closed flux surface with much of the emission coming from the higher density region inside the plasma core making the edge effects less important.

During the X-point phases of the DiMPle pulses when the outer strike point is placed on the horizontal tile 5, then tile 6 and finally the vertical tile 7, the core measurements are again regarded as being more reliable and therefore invest-igated first. Both the KT2 and KT7/2 spectra show that the impurity levels are highest for the tile 6 measurements and lowest for tile 5. This is thought due to more use being made of tile 5, resulting in greater cleaning of this surface. How-ever, it is seen that the impurity levels are much closer than is found for the wall phases. When the low-Z edge emission is considered, the vertical KT7/2 emission again shows the same ordering. However, the KT2 observations show higher intens-ities for the tile 5 phase, with the tile 6 and tile 7 phases tending to overlay. In this case, the larger plasma-outer divertor throat separation in the tile 5 configuration possibly allows higher flows of impurities released in the divertor into the KT2 line-of-sight. In figures 2 and 3, the distance from the inner SOL field line to the divertor throat for the tile 5 configuration is ~8.5 cm, whereas this is only ~3 cm for the tile 6 and tile 7 configurations.

Exceptions to this ordering are found for Ar and He. In the case of Ar, there is a tendency for the KT7/2 tile 5 observations to be higher than those for tile 6 and tile 7, probably due to the rapid cleaning effect of the recently loaded surfaces contam-inating the cleaning plasma. However, it should be emphas-ized that there is extreme variability in the measurements for Ar. For He, the tile 6 and tile 7 KT7/2 measurements overlay, although are seen to be higher than those of tile 5. The same trend can be seen in the KT2 data, although is less marked.

4.7. Impurity concentrations

The use of the same transition for monitoring the mid-Z ele-ments Cr, Fe, Ni and Cu allows estimates of their relative concentrations to be determined given their closeness in Z. These ratios will also apply to the elemental components of radiated power. Table 4 lists the intensities of the mid-Z ele-ments during the five phases of the DiMPle pulses for three pulse ranges, the first corresponding to campaigns C35/C36, the second C36b and the third C38. The relative concentrations were calculated from the outer wall data presented in this table and was found for Cr:Fe:Ni:Cu to be 0.12:0.21:1.0:0.46. The data from this table normalized to the outer wall measurements of each element is shown in figure 25.

Although impurity line intensities have been used in the present study, estimates of the impurity concentrations are of value in order to give context to the results and aid compar-isons with the data from other machines. Whereas the relat-ive concentrations of the mid-Z elements can be determined with reasonable accuracy given that the same transition is used to monitor these elements, it must be recognized that there is a much greater uncertainty in the absolute impurity con-centrations due to uncertainties in the location and therefore parameters of the plasma from where the impurity lines are emitted. These parameters, in any case, are different for the different phases of the DiMPle discharges. Estimates of the maximum impurity concentrations found in the DiMPle pulses are given in table 5. For most of the impurities these have been determined by monitoring changes in the Z effective of the plasma, Z_{eff}, this parameter being defined by

$$Z_{\text{eff}} = \sum_i c_i Z_i^2,$$

where c_i and Z_i are the concentration and atomic number of the *i*th impurity.

In the case of He, VUV spectroscopy showed that for the highest data points the plasma being observed was predominately He. Both changes in the Z_{eff} and pulses in
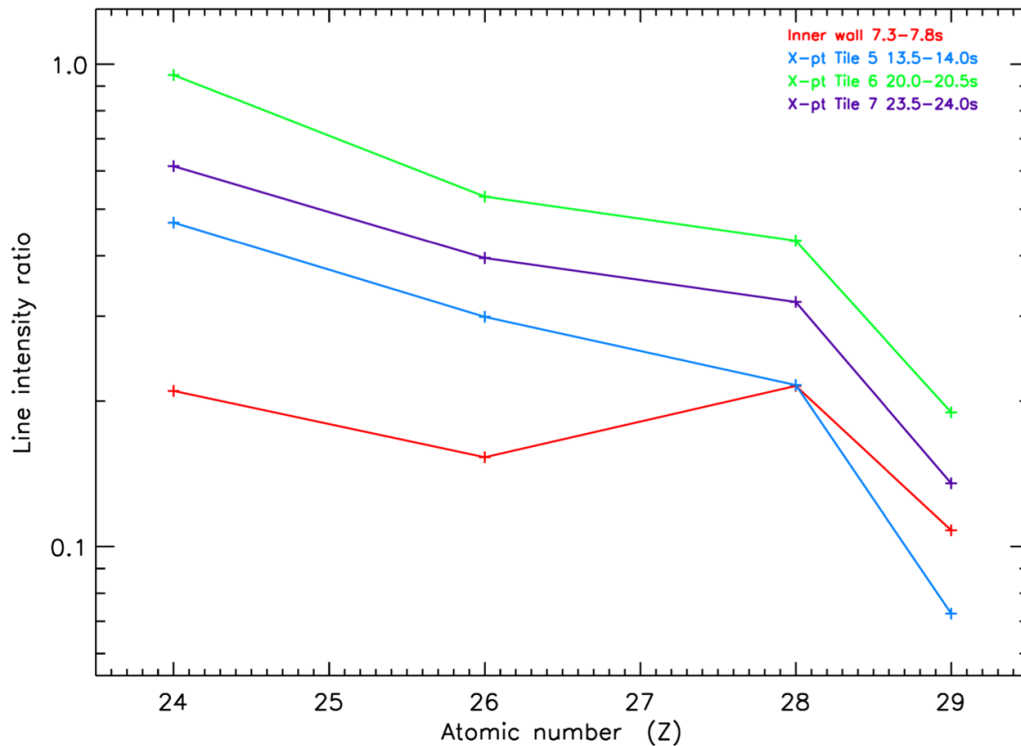
Figure 25. Mid-Z element intensities normalized to those of the outer wall.

Table 5. Estimates of the maximum impurity concentrations found in DiMPle pulses.

Element	Maximum concentration estimate	Element	Maximum concentration estimate
He	5.0e−1	Ar	5.0e−3
Be	1.2e−1	Cr	5.0e−5
C	3.5e−3	Fe	9.0e−5
N	5.0e−2	Ni	4.0e−4
O	9.0e−3	Cu	2.0e−4
Ne	1.0e−2	Mo	5.0e−5
Cl	1.5e−3	W	4.0e−5

which the VUV spectrum showed that Be was the dominant impurity are used for this element. The concentrations for W were found using the W analyzer, which is routinely used on JET to give W concentrations from the features observed at 42–70 Å in the KT7/3 spectrum.

4.8. W emission during DiMPle pulses

Although the KT2 and KT7/3 spectrometers observe somewhat different temperature W UTAs, with the KT2 measurements, particularly the WIK, being the more sensitive, no clear difference in the overall pattern of the measurements is evident given the rather limited data available (Lawson and Coffey 2020). Hence the concern that the heavy W ions move radially outwards due to a centrifugal force (Wesson 1997, Koskela *et al* 2015) leading to their emission falling outside the vertical

KT7 line-of-sight does not appear to be an issue for the DiMPle pulses.

5. Conclusions

An analysis has been made of the behaviour of the most significant impurities seen in the JET DiMPle pulses run during the C35 to C38 campaigns. Although the VUV spectrum allows all significant impurities in JET to be monitored, it does have the disadvantage of being extremely complex given the resolution of the survey instruments used on JET (and other large plasma machines), with many lines being blended. Data recorded by survey spectrometers with a horizontal (KT2) and vertical line-of-sight (KT7) have been used in the analysis. Care has been taken to ensure the reliability of the presented data as much as is possible in an automatic collection of line intensities. These have been checked in particular to ensure that the lowest intensity points do correspond to the expected line.

The DiMPle pulses are ideal both for studying impurity levels when the plasma is placed on different plasma facing surfaces and the longer term behaviour over a number of campaigns. The Be intensities are exceptional amongst the different impurities, being reproducible when the plasma is placed on the outer or inner wall. The other impurities show significant variations. Gases that are introduced into the vessel as a fuel, minority element for ICRH coupling, DMV gas or for particular experiments have high levels following their use. Other impurity elements are retained in the vessel on the plasma facing surfaces. They show a clear systematic behaviour with the plasma positioned on the outer wall and in the

X-point configuration with the outer strike point on tiles 6 and 7 generally having higher impurity levels. This would favour positioning the plasma on the inner rather than outer wall during plasma start-up, particularly in scenarios that move to an early X-point. The generally lower tile 5 impurity levels are thought mainly due to the cleaning effect resulting from the more frequent use of this tile. The impurity levels during the C37, H campaign were lower and this leads to the expectation of higher impurity levels during tritium and deuterium-tritium operations. The metal concentrations during the long restart period before C38 were also depressed. At the same time, the C, O and Cl levels were higher, gradually decaying until steady background levels had been reached. Line-of-sight dependences which affect observations of the lower Z elements monitored by emission from the plasma SOL have been considered in this study.

Data availability statement

All data that support the findings of this study are included within the article (and any supplementary files).

Acknowledgments

ORCID iD

K D Lawson ⬤ https://orcid.org/0000-0002-1251-6392

References

Brezinsek S *et al* 2013 *J. Nucl. Mater.* **438** S303–8
Coenen J W *et al* 2013 *Nucl. Fusion* **53** 073043
Fonck R J, Ramsey A T and Yelle R V 1982 *Appl. Opt.* **21** 2115
Joffrin E *et al* 2019 *Nucl. Fusion* **59** 112021
Koskela T *et al* 2015 *Plasma Phys. Control. Fusion* **57** 045001
Lawson K D and Coffey I H 2020 JET report 'Impurity analysis of JET DiMPle pulses'
Lawson K D and Peacock N J 1980 *J. Phys.* B **13** 3313
Litaudon X *et al* 2017 *Nucl. Fusion* **57** 102001
Matthews G F *et al* 2007 *Phys. Scr.* **T128** 137
Matthews G F *et al* 2013 *J. Nucl. Mater.* **438** S2–10
Matthews G F *et al* 2014 *Phys. Scr.* **T159** 014015
Romanelli F and Laxåback M 2011 *Nucl. Fusion* **51** 094008
Rubel M *et al* 2013 *J. Nucl. Mater.* **438** S1204
Schwob J L, Wouters A W, Suckewer S and Finkenthal M 1987 *Rev. Sci. Instrum.* **58** 1601
Sertoli M *et al* 2015a *J. Nucl. Mater.* **463** 837
Sertoli M *et al* 2015b *J. Nucl. Mater.* **467** 394
Ström P, Petersson P, Rubel M, Fortuna-Zaleśna E, Widdowson A and Sergienko G 2019 *J. Nucl. Mater.* **516** 202
Tolias P, Riva G, De Angeli M, Ratynskaia S, Daminelli G, Lungu C P and Porosnicu C 2018 *Nucl. Mater. Energy* **15** 55
Uccello A, Gervasini G, Ghezzi F, Lazzaro E, Bacharis M, Flanagan J, Matthews G, Järvinen A and Sertoli M 2016 *Phys. Plasmas* **23** 102506
Wesson J A 1997 *Nucl. Fusion* **37** 577
Wolf R C *et al* 1995 JET Preprint JET-P(95)34